Contrib Mineral Petrol (2013) 165:1195–1224
DOI 10.1007/s00410-013-0854-9

Partial melting of lower crust at 10–15 kbar: constraints on adakite and TTG formation

Qing Qian · Jörg Hermann

Received: 21 September 2012 / Accepted: 12 January 2013 / Published online: 3 February 2013

Abstract The pressure–temperature (*P–T*) conditions for producing adakite/tonalite–trondhjemite–granodiorite (TTG) magmas from lower crust compositions are still open to debate. We have carried out partial melting experiments of mafic lower crust in the piston-cylinder apparatus at 10–15 kbar and 800–1,050 °C to investigate the major and trace elements of melts and residual minerals and further constrain the *P–T* range appropriate for adakite/TTG formation. The experimental residues include the following: amphibolite (plagioclase + amphibole ± garnet) at 10–15 kbar and 800 °C, garnet granulite (plagioclase + amphibole + garnet + clinopyroxene + orthopyroxene) at 12.5 kbar and 900 °C, two-pyroxene granulite (plagioclase + clinopyroxene + orthopyroxene ± amphibole) at 10 kbar and 900 °C and 10–12.5 kbar and 1,000 °C, garnet pyroxenite (garnet + clinopyroxene ± amphibole) at 13.5–15 kbar and 900–1,000 °C, and pyroxenite (clinopyroxene + orthopyroxene) at 15 kbar and 1,050 °C. The partial melts change from granodiorite to tonalite with increasing melt proportions. Sr enrichment occurs in partial melts in equilibrium with <20 wt% plagioclase, whereas depletions of Ti, Sr, and heavy rare earth elements (HREE) occur relative to the starting material when the amounts of residual amphibole, plagioclase, and garnet are >20 wt%, respectively. Major elements and trace element patterns of partial melts produced by 10–40 wt% melting of lower crust composition at 10–12.5 kbar and 800–900 °C and 15 kbar and 800 °C closely resemble adakite/TTG rocks. TiO_2 contents of the 1,000–1,050 °C melts are higher than that of pristine adakite/TTG. In comparison with natural adakite/TTG, partial melts produced at 10–12.5 kbar and 1,000 °C and 15 kbar and 1,050 °C have elevated HREE, whereas partial melts at 13.5–15 kbar and 900–1,000 °C in equilibrium with >20 wt% garnet have depressed Yb and elevated La/Yb and Gd/Yb. It is suggested that the most appropriate *P–T* conditions for producing adakite/TTG from mafic lower crust are 800–950 °C and 10–12.5 kbar (corresponding to a depth of 30–40 km), whereas a depth of >45–50 km is unfavorable. Consequently, an overthickened crust and eclogite residue are not necessarily required for producing adakite/TTG from lower crust. The lower crust delamination model, which has been embraced for intra-continental adakite/TTG formation, should be reappraised.

Keywords Partial melting experiment · Lower continental crust · Adakite · TTG · Trace element

Communicated by J. Hoefs.

Electronic supplementary material The online version of this article (doi:10.1007/s00410-013-0854-9) contains supplementary material, which is available to authorized users.

Q. Qian (✉)
Key Laboratory of Mineral Resources, Institute of Geology and Geophysics, Chinese Academy of Sciences, Beijing 100029, China
e-mail: qianqing@mail.iggcas.ac.cn

Q. Qian · J. Hermann
Research School of Earth Sciences, The Australian National University, Canberra, ACT 0200, Australia

Introduction

Adakite and Archean TTG (tonalite, trondhjemite, and granodiorite) are silicic to intermediate igneous rocks that are geochemically characterized by high Al_2O_3, Sr and Ba, low Y and heavy rare earth elements (REE), strong depletion of high-field-strength elements (HFSE) such as Nb, Ta, and Ti, and lack of negative Sr and Eu anomalies (Martin 1986, 1999; Defant and Drummond 1990; Martin

et al. 2005). Cenozoic adakites mostly occur in the circum-Pacific arcs and are widely believed to have formed by partial melting of hot subducted oceanic crust in the stability field of eclogite or garnet amphibolite (Kay 1978; Defant and Drummond 1990; Sajona et al. 1993; Morris 1995; Stern and Kilian 1996; Beate et al. 2001). A slab-melting petrogenesis has also been proposed for Archean TTG rocks (Martin 1986, 1987, 1999; Drummond and Defant 1990; Foley et al. 2002; Martin and Moyen 2002; Martin et al. 2005), which generally possess lower MgO, Cr, and Ni than modern adakites probably due to little interaction between the Archean slab-melts and mantle wedge (Martin 1999; Martin et al. 2005).

Recent studies have shown that adakites/TTG magmas are not confined to arc settings and can alternatively be generated by partial melting of mafic lower crust. For example, Cenozoic adakites of a post-collisional extensional setting crop out sparsely within a ~1,500 km magmatic belt in southern Tibet (Chung et al. 2003; Hou et al. 2004; Guo et al. 2007). Mesozoic adakites related to an intra-continental extensional setting occur in a wide area of more than 1,000,000 square kilometers in the eastern part of China (e.g., Zhang et al. 2001; Gao et al. 2004; Wang et al. 2006; Xu et al. 2002, 2006, 2008, 2010; Liu et al. 2010; Qian and Hermann 2010). Even in the circum-Pacific arcs (e.g., Cordillera Blanca, Peruvian Andes), some of the Cenozoic adakites were interpreted to be generated from partial melting of mafic lower crust (Atherton and Petford 1993; Petford and Atherton 1996; Coldwell et al. 2011). Although these adakites generally have higher K_2O/Na_2O (>0.5) and much more enriched Sr–Nd–Hf isotopes compared to the circum-Pacific arc adakites likely formed by partial melting of subducted slab, they are similar in most of the major and trace element features. This led Defant et al. (2002) to modify their original definition of adakite, by emphasizing that "the term adakite should not be restricted to processes related only to slab melting but must include those involving the melting of the lower crust". Archean TTG may also be formed by anatexis of mafic lower crust in tectonically or magmatically thickened arc systems or oceanic plateaus (de Wit 1998; Smithies 2000; Zegers and van Keken 2001; Rapp et al. 2003; Smithies et al. 2003, 2009; Condie 2005; Bedard 2006). Recent hafnium and oxygen isotopes coupled with precise zircon U–Pb dating demonstrate that some of the TTG rocks represent crust reworking through anatexis of pre-existing mafic lower crust (Whalen et al. 2002; Kemp et al. 2006; Jahn et al. 2008; Jiang et al. 2010; Rollinson 2012). This petrogenesis is able to explain the low MgO, Cr, and Ni features of TTG rocks (Smithies 2000; Condie 2005).

The pressure–temperature (*P–T*) range for producing adakite/TTG magmas from mafic sources remains a matter of considerable debate. Tonalitic, trondhjemitic, and granodioritic melts were produced in dehydration-melting of natural amphibolites and synthetic basalts at 1–6.9 kbar (Beard and Lofgren 1991), 8 kbar (Rushmer 1991), 10 kbar (Wyllie and Wolf 1993; Wolf and Wyllie 1994), 15–25 kbar (Clemens et al. 2006; Xiao and Clemens 2007; Coldwell et al. 2011), and 5–30 kbar (Winther and Newton 1991; Winther 1996). However, major elements of the melts provide poor constraints on melting conditions of adakite/TTG magma. The Sr enrichment and Y and heavy rare earth element (HREE) depletions of adakite/TTG rocks led to the general belief that partial melting occurs in the stability field of garnet amphibolite, garnet granulite, or elcogite, leaving a residue with garnet and amphibole and minor plagioclase (Arth and Hanson 1972; Martin 1986, 1999; Defant and Drummond 1990; Peacock et al. 1994; Condie 2005). A minimum pressure of ~15 kbar is consistently indicated by geochemical modeling utilizing Sr/Y ratio (Moyen 2009) and by a series of partial melting experiments employing trace element analysis for adakite/TTG melts from MORB (mid-ocean ridge basalt), shoshonite or Archean greenstones (Rapp et al. 1991; Sen and Dunn 1994; Rapp 1995; Rapp and Watson 1995; Xiong et al. 2005, 2009; Clemens et al. 2006; Xiong 2006; Nair and Chacko 2008; Adam et al. 2012). Partial melts produced at 19–40 kbar from eclogitic MORBs closely resemble adakite/TTG in trace elements (Rapp et al. 1999, 2003; Laurie and Stevens 2012). In order to form the strong HFSE and HREE depletions of partial melts, it is suggested that rutile and high amounts of garnet are required to be stable in the residue (Xiong et al. 2005, 2009; Xiong 2006; Nair and Chacko 2008).

While formation of adakite/TTG melts in a subduction setting has attracted significant attention, only few studies have been conducted to investigate the partial melting of lower continental crust as source for these melts. The lower continental crust has a major and trace element content quite different to MORB, and thus, it is not a priori clear whether partial melting under eclogite facies conditions is required to produce adakite/TTG magmas. Geochemical modeling of Moyen (2009) indicates that the pressure of adakite/TTG generation from mafic lower crust with elevated Sr/Y ratio (~15) cannot be higher than 10 kbar. Geochemical modeling of Nagel et al. (2012) indicates that trace elements of TTG can be achieved by partial melting of tholeiitic island-arc crust at 10–14 kbar. Springer and Seck (1997) observed that partial melts of lower crust granulites at 15 kbar have modeled HREE depressed well below the level of natural tonalites and proposed that the suitable pressure for producing TTG from mafic granulite is 10–12.5 kbar. In contrast, the partial melting experiments of Adam et al. (2012) show that TTG may be selectively derived from arc-like mafic rocks at depths of

15–30 kbar. In practice, however, lots of studies have relied on the MORB-melting experimental results to interpret the production of adakite/TTG with geological, geochronological, and/or isotopic evidences indicating a potential origin of lower crust. This limitation resulted in specific geological models such as crustal overthickening and lower crust delamination. It is thus meaningful to determine experimentally the appropriate *P–T* conditions for the formation of adakite/TTG from lower continental crust.

In this paper, we present the results of partial melting experiments at 10–15 kbar and 800–1,050 °C on a synthetic, trace element doped starting material resembling the lower crust compositions of Rudnick and Gao (2003) (RG2003) and Condie and Selverstone (1999) (CS1999) in major elements (Table 1). The main aim is to investigate the major and trace element compositions of partial melts from anatexis of mafic lower crust as a function of residual phase assemblages. The experimental results were used to constrain the *P–T* conditions of adakite/TTG formation from mafic lower crust and to provide geological implications with emphasis on whether an overthickened crust is necessary to produce adakite/TTG magmas in such a tectonic setting.

Experimental technique

Starting material

The starting material (Table 1) is in major elements close to the average lower continental crust estimated by Rudnick and Gao (2003) and Condie and Selverstone (1999). Sr, Y, and Zr are very similar to the lower crustal composition given by Rudnick and Gao (2003), whereas REE have been elevated in order to facilitate analysis (Table 1). A silica gel doped with trace elements (mostly between 30 and 1,300 ppm) was mixed with analytical grade TiO_2, MnO, MgO, and P_2O_5 and appropriate amounts of $CaCO_3$, Na_2CO_3, and K_2CO_3. The compound was finely milled under acetone using an agate mill and pestle, tightly pressed, and heated overnight at 1,000 °C to extract the CO_2 component. Iron was added to the decarbonated compound in the form of fayalite, which had been synthesized by the reaction of pure SiO_2 and Fe_2O_3 under the N–NO_3 buffer. The compound was then divided into two parts to make an anhydrous Mix A and a hydrous Mix B (H_2O ~8.25 wt%) by adding Al_2O_3 and $Al(OH)_3$, respectively. Anhydrous major and trace elements of Mix A and Mix B were analyzed on glasses of their aliquots which were fused at ~1,400 °C on a molybdenum strip. The two mixtures contain identical abundances of anhydrous oxides and trace elements within analytical error

Table 1 Chemical analyses of the starting material (Mix A and B)

	Mix A	Mix B	RG2003	CS1999
Major elements (wt%)				
n	7	6		
SiO_2	53.31 (0.72)	48.55 (1.33)	53.4	53.18
TiO_2	1.21 (0.06)	1.14 (0.12)	0.82	0.96
Al_2O_3	17.00 (0.44)	15.22 (0.77)	16.9	16.59
FeO	8.37 (0.21)	8.15 (0.66)	8.57	9.60
MnO	0.02 (0.01)	0.05 (0.04)	0.10	0.16
MgO	7.27 (0.18)	6.77 (0.36)	7.24	6.10
CaO	9.40 (0.17)	8.90 (0.31)	9.59	8.59
Na_2O	2.58 (0.04)	2.35 (0.12)	2.65	3.23
K_2O	0.60 (0.05)	0.50 (0.07)	0.61	1.38
P_2O_5	0.25 (0.04)	0.15 (0.03)	0.10	0.22
H_2O	–	8.25	–	–
Total	100.00	100.00	99.98	100.00
Mg#	0.61	0.60	0.60	0.53
Trace elements (ppm)				
n	6	6		
Li	27.0 (0.6)	28.6 (0.9)	13	–
Sc	24.1 (1.2)	23.5 (1.6)	31	28.3
V	67.9 (4.4)	71.4 (7.5)	196	–
Cr	19.2 (5.1)	18.9 (6.6)	215	133
Rb	45.0 (3.4)	42.3 (5.6)	11	36.8
Sr	323 (10)	338 (13)	348	518
Y	18.1 (1.8)	17.0 (1.5)	16	25.3
Zr	78.3 (4.3)	75.2 (5.9)	68	86
Nb	74.9 (3.2)	75.6 (5.2)	5	7.75
Cs	41.4 (2.7)	39.7 (3.1)	0.3	–
Ba	629 (12)	637 (19)	259	564
La	38.6 (1.7)	39.4 (3.1)	8	21.6
Ce	66.7 (2.6)	69.3 (5.6)	20	46.4
Pr	37.4 (1.6)	38.1 (3.0)	2.4	–
Nd	39.7 (2.1)	40.4 (3.7)	11	23.5
Sm	37.5 (2.3)	37.1 (2.7)	2.8	5.17
Eu	37.2 (2.0)	38.7 (2.1)	1.1	1.30
Gd	33.7 (2.6)	34.5 (2.7)	3.1	4.67
Dy	35.1 (1.8)	35.4 (3.6)	3.1	–
Er	16.4 (1.2)	16.5 (1.6)	1.9	–
Yb	17.5 (0.9)	17.8 (1.2)	1.5	2.09
Lu	16.8 (1.0)	16.9 (1.3)	0.25	0.37
Hf	19.4 (1.5)	18.5 (1.2)	1.9	1.90
Ta	25.5 (2.0)	25.0 (1.5)	0.6	0.50
Pb	76.1 (27.0)	63.2 (13.5)	4	9.8
Th	17.9 (1.5)	17.3 (1.4)	1.2	1.64
U	23.6 (1.0)	24.2 (1.3)	0.2	1.38

Trace elements of Mix A and B are on an anhydrous basis. RG2003 and CS1999 (normalized to 100 %) are lower continental crust of Rudnick and Gao (2003) and Condie and Selverstone (1999), respectively. Mg# = Mg/(Mg + Fe^T). Units in parentheses indicate standard deviation (1σ) from average analyses. *n* number of analysis

Table 2 Run conditions and phase proportions (wt%)

Run no.	*P* (kbar)	*T* (°)	H_2O (wt%)	Time	Melt	Gt	Amp	Cpx	Opx	Pl	Accessory phases
C-3161	10	800	6.0	A week	23 (27)	–	61	–	–	16	Ilm
C-3179	10	900	4.0	A week	27 (26)	–	24	12	10	27	Ilm, Ap
C-3081	10	1,000	1.8	A week	13 (20)	–	–	22	17	48	Ilm, Rt
C-3180	12.5	800	4.0	A week	14 (15)	–	64	–	–	22	
C-3124	12.5	900	4.0	A week	39 (34)	11	20	18	2	10	Rt
C-3136	12.5	1,000	2.0	A week	33 (35)	–	–	20	17	30	Rt
C-3221	13.5	900	4.0	A week	44 (43)	25	18	13	–	–	
C-3171	15	800	4.0	A week	27 (29)	2	62	–	–	9	Ap, Rt, Tit, All
C-3162	15	900	6.0	A week	40 (45)	30	10	20	–	–	Rt
C-3052	15	1,000	1.5	A week	44 (32)	30	–	26	–	–	Ap
C-3217	15	1,000	2.0	A week	59 (52)	21	–	20	–	–	
C-3123	15	1,050	2.0	A week	69 (60)	–	–	24	7	–	

Phase proportions were estimated by mass balance. Numbers in parentheses represent melt proportions estimated by assuming $D_{Cs}^{bulk} = 0$. Carbon spheres were used in all runs except C-3052 to trap the partial melts. –, not stable

(Table 1). H_2O amounts of the starting material were controlled by blending Mix A and Mix B in various proportions. For experiments at 1,000 °C, the H_2O content is ≤2 wt%, only slightly elevated with respect to a subsolidus amphibolite. At lower temperatures, we increased the water content in order to obtain a melt fraction of 20–30 % (Table 2) and large enough melt pools for trace element analyses. Such elevated melt fractions help to promote equilibration at lower temperature. The extent of melting is not large enough to exhaust the main minerals amphibole or plagioclase.

Experimental procedure

The partial melting experiments were conducted in a conventional 1/2-inch end-loaded piston-cylinder apparatus (Hibberson 1978) at the Research School of Earth Sciences (RSES), Australian National University (ANU). About 20 mg starting material was packed into a gold capsule with an outside diameter of 2.3 mm. 1–2 mg carbon spheres of 80 μm diameter were loaded above the starting material in the capsule to trap partial melts. No carbon spheres were added in run C-3052, which was conducted at the same *P–T* condition with C-3217. The gold capsule was sealed by arc welding, during which it was wrapped in a water-soaked tissue paper to prevent water loss. The furnace assembly was composed of Teflon foil, compressed pure NaCl and Pyrex sleeves, graphite heater, and sintered MgO spacer at the center of which the gold capsule was embedded. Temperature was controlled and measured with type B thermocouple ($Pt_{94}Rh_6/Pt_{70}Rh_{30}$), which was protected by two bore mullite tubes and placed vertically above the capsule in the central part of the NaCl/Pyrex/MgO assembly. A 1-mm thick MgO disk was inserted between the thermocouple end-point and the gold capsule to avoid reaction between them. Precision of the thermocouple is better than ±2 °C and accuracy is within ±10 °C. No friction correction was applied, and pressure measured by load on the piston is believed to be accurate to within ±0.1 GPa (Hermnan and Green 2001). The oxygen fugacity was controlled by the presence of graphite around and within the capsule as graphite spheres, leading to f_{O_2} conditions about 2 log units below QFM (Bottazzi et al. 1999). We noticed a limited loss of iron during the experiments. Mass balance calculation shows that Fe loss was up to 25 % in runs with T ≥1,000 °C, and <15 % in the other runs. The experiments were run at 10–15 kbar and 750–1,050 °C for 1 week (~168 h) and were quenched to below 70 °C within 5 s by terminating the power. The retrieved capsules were exposed vertically by grinding on sand paper, mounted in epoxy, and polished on diamond laps.

Analytical methods

Major elements of the product minerals and quenched melts were measured by quantitative energy dispersive X-ray spectroscopy (EDS) using a JEOL 6400 scanning

Fig. 1 Backscattered electron (BSE) photomicrographs of run products. **a** run C-3161 (10 kbar, 800 °C); **b** run C-3179 (10 kbar, 900 °C); **c** run C-3081 (10 kbar, 1,000 °C); **d** run C-3124 (12.5 kbar, 900 °C), pyroxenes and plagioclase are mostly less than 10 μm in size; **e** run C-3136 (12.5 kbar, 1,000 °C); **f** run C-3221 (13.5 kbar, 900 °C); **g** run C-3171 (15 kbar, 800 °C); **h** run C-3162 (15 kbar, 900 °C); **i** run C-3052 (15 kbar, 1,000 °C), *black spots* on garnet were left by LA-ICP-MS analysis; **j** run C-3123 (15 kbar, 1,050 °C). *Amp* amphibole, *Cpx* clinopyroxene, *Gt* garnet, *Opx* orthopyroxene, *Pl* plagioclase, *All* allanite, *Ap* apatite, *Ilm* ilmenite, *Rt* rutile, *Tit* titanite ▶

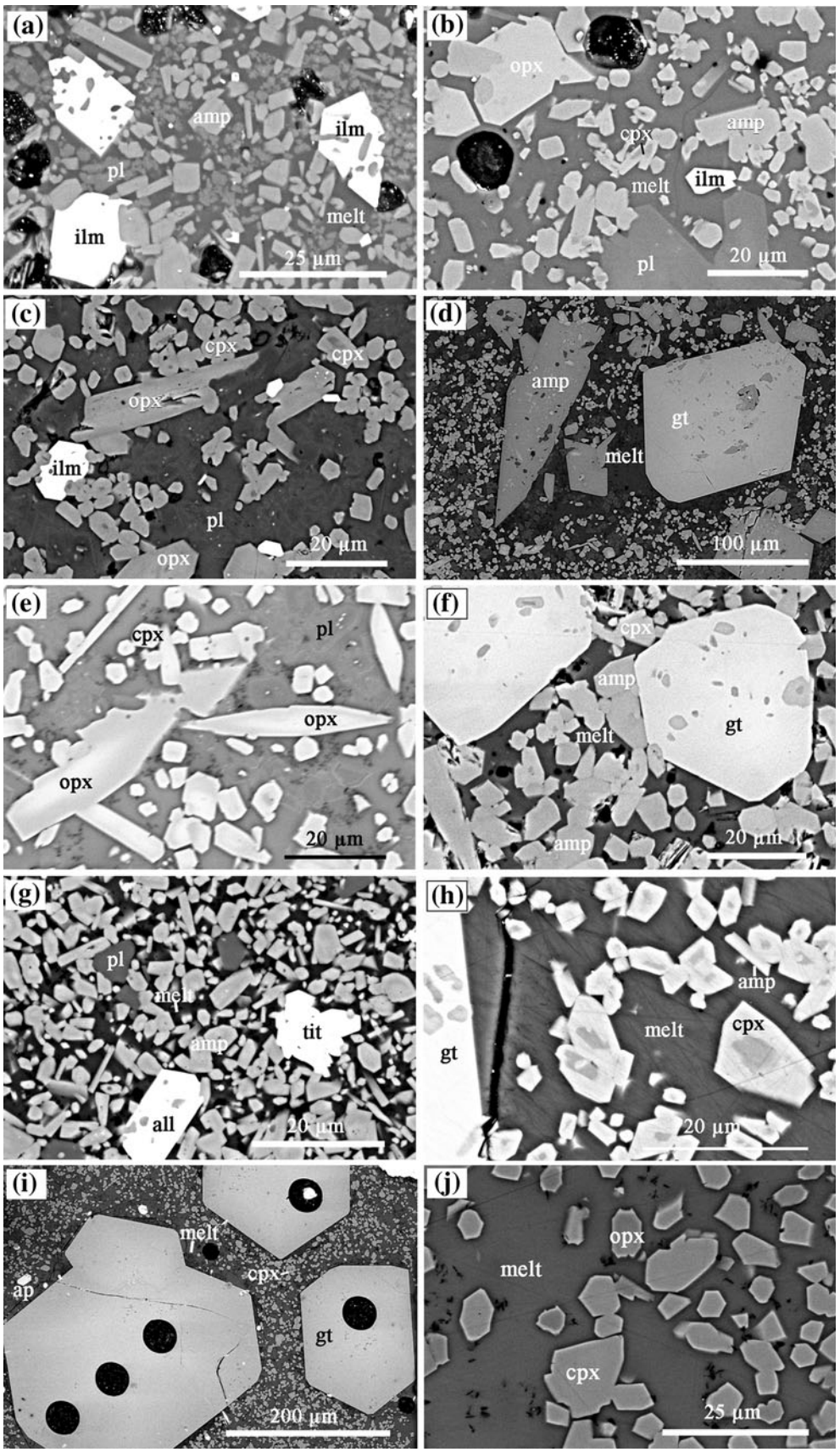
(a)
amp
ilm
pl
melt
ilm
25 µm
(b)
opx
cpx
amp
melt
ilm
pl
20 µm
(c)
cpx
cpx
opx
ilm
pl
opx
20 µm
(d)
amp
gt
melt
100 µm
(e)
cpx
pl
opx
opx
20 µm
(f)
cpx
amp
melt
gt
amp
20 µm
(g)
pl
melt
tit
amp
all
20 µm
(h)
amp
melt
cpx
gt
20 µm
(i)
melt
cpx
ap
gt
200 µm
(j)
opx
melt
cpx
25 µm

electron microscope (SEM) at the Electron Microprobe Unit (EMU), ANU. The accelerating voltage, beam current, and counting time were 15 kV, 1 nA, and 120 s, respectively. For mineral analyses, a focussed beam was used. The glass was measured by scan analyses over an area of 10 × 10 μm to minimize alkali (mainly Na) loss as a result of electron bombardment. Phase relations were determined by back-scattered electron (BSE) imaging during the analyses, and high-resolution BSE images were taken with a Hitachi 4300 SEM at EMU. Representative BSE photomicrographs of the experimental products are illustrated in Fig. 1.

Trace elements of the quenched melts and minerals >30 μm in size were analyzed by laser ablation inductively coupled plasma mass spectrometry (LA-ICP-MS) at RSES, using an Agilent 7500 coupled to a pulsed 193 nm ArF Excimer laser operating at a repetition rate of 5 Hz. A circular beam of 22 μm was used. The counting times were 20 and 40 s for background and analysis, respectively. The synthetic NIST 612 glass (Pearce et al. 1997) was used as an external standard, and ^{29}Si was taken as an internal standard with absolute SiO_2 values determined by EDS. Accuracy and reproducibility were monitored by replicate analyses of the secondary standard BCR-2G glass and were better than 10 %.

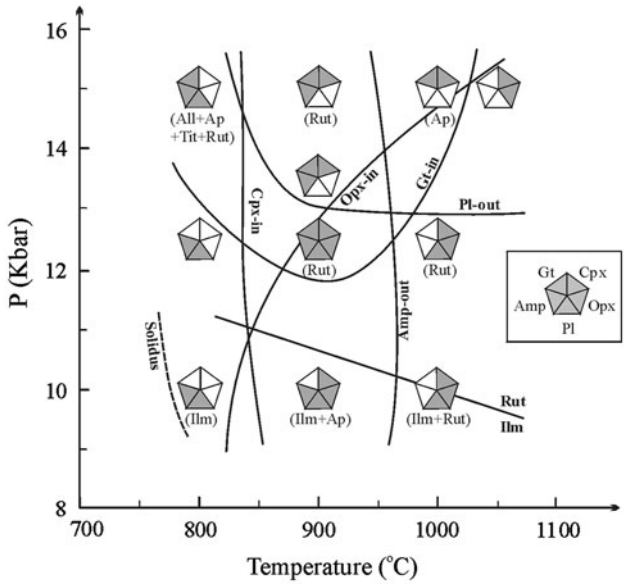

Fig. 2 Phase assemblages of the experimental runs and limits of stability of major phases. Stable accessory phases are shown in *brackets*. The effective solidus (*dashed line*) is confined to between 750 and 800 °C at 10 kbar

Experimental results

Phase assemblages

Mineral assemblages and phase proportions at different run conditions are presented in Table 2. 1.5–2.0 wt% H_2O was contained in the starting material of the 1,000–1,050 °C experiments, close to the water content (~1.25 wt%) of an amphibolite with ~50 % amphibole crystals. The 800–900 °C experiments with 4–6 wt% H_2O contained excess water, resulting in a similar amount of partial melt. The product minerals are euhedral to subhedral (Fig. 1). Garnet varies about 25–250 μm in diameter. Other minerals are mostly 2–30 μm in size, except that a few

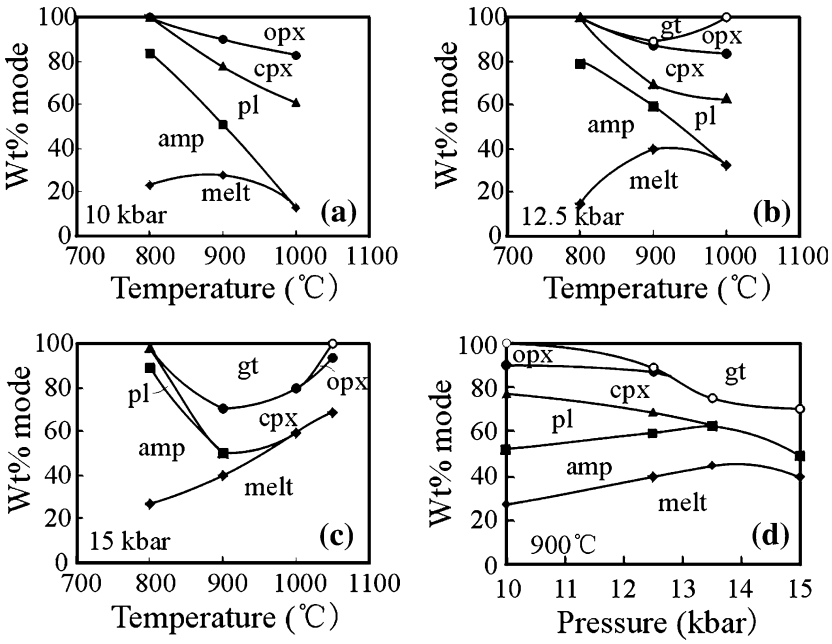

Fig. 3 Modes of run products (obtained by mass balance) plotted versus temperature at 10 kbar (**a**), 12.5 kbar (**b**) and 15 kbar (**c**) and pressure at 900 °C (**d**). It should be noted that phase proportions also depend on the H_2O content, which was increased in the low temperature runs in order to keep the amount of melt ≥15 %

Table 3 Major elements of minerals

Run no.	*n*	Phase	SiO_2	TiO_2	Al_2O_3	FeO	MnO	MgO	CaO	Na_2O	K_2O	P_2O_5	Total
C-3161	4	Pl	50.23 (1.42)	0.09 (0.07)	31.62 (1.40)	0.82 (0.13)	n.d.	0.24 (0.10)	14.51 (1.61)	2.34 (0.76)	0.14 (0.04)	0.13 (0.07)	100.13
	5	Amp	45.77 (1.45)	1.72 (0.25)	13.18 (1.07)	12.49 (1.24)	n.d.	11.77 (0.82)	11.17 (0.54)	1.76 (0.08)	0.34 (0.08)	n.d.	98.21
C-3179	6	Pl	51.69 (1.14)	n.d.	30.27 (0.63)	0.35 (0.17)	n.d.	0.10 (0.04)	13.02 (0.82)	3.85 (0.44)	n.d.	n.d.	99.30
	8	Amp	43.63 (1.21)	2.16 (0.35)	13.61 (0.89)	11.71 (0.74)	n.d.	13.31 (0.66)	10.26 (0.47)	2.10 (0.15)	0.31 (0.05)	n.d.	97.08
	6	Cpx	51.45 (0.39)	0.68 (0.14)	3.87 (0.82)	10.08 (0.19)	n.d.	13.61 (0.41)	18.80 (0.49)	0.54 (0.10)	n.d.	n.d.	99.02
	7	opx	50.94 (0.65)	0.36 (0.05)	4.05 (0.63)	20.67 (0.63)	n.d.	21.05 (0.77)	1.68 (0.28)	0.21 (0.08)	n.d.	n.d.	98.96
C-3081	6	Pl	55.55 (0.89)	0.23 (0.22)	26.96 (0.93)	0.83 (0.33)	n.d.	0.29 (0.18)	10.17 (0.92)	4.93 (0.50)	0.42 (0.09)	n.d.	99.37
	4	cpx	50.45 (0.35)	1.45 (0.17)	6.30 (0.92)	9.38 (0.67)	n.d.	13.53 (1.07)	18.10 (0.62)	0.70 (0.14)	n.d.	n.d.	99.91
	5	opx	52.48 (1.13)	0.57 (0.07)	4.76 (0.42)	17.38 (1.29)	n.d.	23.00 (0.82)	1.82 (0.26)	0.36 (0.12)	n.d.	n.d.	100.38
C-3180	6	Pl	55.32 (1.96)	n.d.	27.73 (0.97)	0.25 (0.23)	n.d.	0.08 (0.05)	10.06 (1.36)	5.52 (0.79)	0.16 (0.05)	n.d.	99.15
	6	Amp	43.20 (0.70)	1.92 (0.15)	13.86 (1.56)	14.80 (2.14)	n.d.	11.04 (0.52)	10.06 (0.62)	1.86 (0.09)	0.32 (0.03)	n.d.	97.04
C-3124	7	Pl	51.37 (1.73)	0.13 (0.09)	30.62 (1.85)	0.48 (0.18)	n.d.	0.17 (0.10)	12.92 (1.10)	3.58 (0.64)	0.15 (0.04)	n.d.	99.43
	5	Amp	41.51 (0.42)	3.49 (0.11)	15.52 (0.33)	11.36 (0.84)	n.d.	12.61 (0.59)	10.17 (0.21)	2.33 (0.05)	0.42 (0.04)	n.d.	97.41
	7	Gt	39.46 (0.44)	1.38 (0.23)	21.37 (0.54)	18.52 (0.95)	n.d.	11.61 (0.71)	7.43 (0.22)	0.07 (0.04)	n.d.	n.d.	99.85
	5	Cpx	50.05 (0.50)	1.17 (0.04)	6.58 (0.80)	8.92 (0.75)	n.d.	13.41 (0.61)	19.29 (0.81)	0.65 (0.17)	n.d.	n.d.	100.07
	5	Opx	51.46 (1.02)	0.42 (0.07)	6.22 (0.47)	17.64 (1.43)	n.d.	21.90 (1.41)	1.56 (0.30)	0.22 (0.18)	n.d.	n.d.	99.43
C-3136	7	Pl	52.07 (1.27)	0.37 (0.25)	28.53 (1.67)	0.97 (0.48)	n.d.	0.44 (0.33)	12.20 (1.30)	3.63 (0.28)	0.25 (0.08)	n.d.	98.46
	4	Cpx	49.37 (0.51)	1.31 (0.16)	7.86 (0.40)	8.01 (1.11)	n.d.	14.16 (0.41)	18.41 (0.84)	0.63 (0.04)	n.d.	n.d.	99.73
	4	Opx	50.89 (0.98)	0.54 (0.20)	6.83 (0.30)	16.59 (1.22)	n.d.	23.28 (0.25)	1.70 (0.42)	0.23 (0.19)	n.d.	n.d.	100.06
C-3221	9	Gt	39.10 (0.53)	1.07 (0.32)	21.45 (0.30)	19.69 (0.76)	n.d.	9.39 (0.72)	8.94 (0.29)	0.16 (0.04)	n.d.	0.11 (0.07)	99.91
	9	Amp	43.49 (0.51)	1.84 (0.07)	14.42 (0.52)	11.54 (0.49)	n.d.	13.33 (0.42)	10.76 (0.23)	2.27 (0.12)	0.37 (0.04)	n.d.	98.01
	6	Cpx	50.92 (0.75)	0.80 (0.13)	5.96 (1.32)	7.56 (0.51)	n.d.	13.03 (0.88)	20.19 (1.12)	0.69 (0.20)	n.d.	n.d.	99.14
C-3171	7	Pl	54.00 (1.71)	0.05 (0.05)	29.23 (1.00)	0.27 (0.23)	n.d.	n.d.	11.77 (1.20)	4.46 (0.93)	0.13 (0.04)	n.d.	100.00
	7	Amp	44.58 (1.92)	1.69 (0.09)	15.81 (1.45)	12.54 (1.29)	n.d.	10.86 (1.32)	11.18 (1.23)	1.96 (0.16)	0.40 (0.07)	n.d.	99.03
	6	Gt	37.68 (0.42)	0.93 (0.10)	21.03 (0.68)	22.03 (0.43)	0.13 (0.10)	6.12 (0.39)	9.96 (0.18)	0.17 (0.04)	n.d.	0.16 (0.05)	98.04
C-3162	6	Amp	43.06 (0.72)	2.08 (0.19)	16.20 (0.30)	12.08 (0.80)	n.d.	12.30 (0.30)	10.54 (0.09)	2.35 (0.06)	0.38 (0.06)	n.d.	98.99
	8	Gt	39.06 (0.44)	1.25 (0.12)	21.10 (0.26)	19.79 (0.79)	n.d.	10.20 (0.63)	8.68 (0.47)	0.18 (0.04)	n.d.	0.20 (0.04)	100.47
	3	Cpx	51.00 (0.82)	1.14 (0.13)	10.26 (0.67)	7.53 (0.25)	n.d.	10.27 (0.85)	17.60 (0.97)	1.13 (0.05)	n.d.	0.11 (0.06)	99.05
C-3052	19	Gt	39.31 (0.64)	1.37 (0.42)	21.49 (0.51)	17.72 (1.25)	n.d.	11.93 (0.80)	7.32 (0.28)	0.11 (0.05)	n.d.	0.23 (0.10)	99.48
	7	Cpx	50.73 (0.81)	1.19 (0.10)	10.00 (0.26)	6.78 (0.43)	n.d.	11.84 (0.48)	17.78 (0.55)	1.43 (0.13)	n.d.	0.16 (0.07)	99.91
C-3217	6	Gt	40.44 (0.42)	0.69 (0.40)	22.40 (0.36)	15.92 (0.49)	n.d.	13.73 (0.88)	6.97 (0.87)	0.10 (0.06)	n.d.	n.d.	100.23
	5	Cpx	50.95 (0.27)	0.86 (0.11)	6.43 (1.26)	6.12 (0.11)	n.d.	14.34 (0.67)	19.48 (0.62)	0.80 (0.08)	n.d.	n.d.	98.97
C-3123	5	Cpx	48.58 (0.48)	1.12 (0.07)	11.22 (0.82)	6.35 (0.42)	n.d.	13.13 (0.57)	18.08 (0.45)	0.85 (0.20)	n.d.	n.d.	99.33
	5	opx	50.46 (0.56)	0.44 (0.04)	9.73 (0.74)	12.95 (1.21)	n.d.	24.23 (0.83)	1.80 (0.31)	0.33 (0.18)	n.d.	n.d.	99.94

Numbers in parentheses refer to standard deviation (1σ) of multiple analyses. *n.d.* not detected

plagioclase, orthopyroxene, and amphibole crystals reach 30–100 μm. The quenched melts are distributed among residual minerals or carbon spheres at the top of the capsule. Melt proportions were estimated by mass balance and alternatively by assuming that Cs is completely incompatible and only hosted in the melt. The results from both approaches are in good agreement (Table 2, Electronic Appendix 1a). The proportion of melt varies from 13 to 69 wt%, showing an increase with temperature and H_2O content (Electronic Appendix 1b). Since no melt was produced in an additional fluid-present experiment at 10 kbar and 750 °C, the solidus temperature was constrained to lie between 750 and 800 °C at 10 kbar and 6 wt% H_2O.

The stability of mineral phases in the *P–T* space is illustrated in Fig. 2. The partial melting residues are as follows: amphibolite (amphibole + plagioclase ± garnet) at 10–15 kbar and 800 °C, garnet granulite (plagioclase + amphibole + clinopyroxene + orthopyroxene + garnet) at 12.5 kbar and 900 °C, two-pyroxene granulite (plagioclase + clinopyroxene + orthopyroxene ± amphibole) at 10 kbar and 900 °C and 10–12.5 kbar and 1,000 °C, garnet pyroxenite (garnet + clinopyroxene ± amphibole) at 13.5–15 kbar and 900–1,000 °C, and pyroxenite (clinopyroxene + orthopyroxene) at 15 kbar and 1,050 °C. Garnet was present in small amounts at 15 kbar but was absent at 10–12.5 kbar under 800 °C, probably due to the reluctance of garnet nucleation below 900 °C (Wyllie and Wolf 1993; Wolf and Wyllie 1994). Garnet has a maximum proportion of 11 and 30 % at 12.5 and 15 kbar, respectively, at 900 °C (Fig. 3b, c). Garnet increases in proportion while plagioclase and orthopyroxene decrease with increasing pressure. With increasing temperature, amphibole decreases whereas clinopyroxene and orthopyroxene increase (Fig. 3). The stability of amphibole and clinopyroxene is not sensitive to pressure variation in the experimental *P–T* range. The exact phase proportions are not only a function of pressure and temperature but will also depend on H_2O content. Generally, higher water contents result in a lower amount of amphibole and plagioclase. However, the increased degree of melting due to the elevated water contents at low temperatures was not high enough to exhaust these phases and thus severely affect the phase relations of the major minerals. Ilmenite is stable at 10 kbar and 800–1,000 °C, and rutile becomes stable at 10 kbar and 1,000 °C, 12.5 kbar and 900–1,000 °C and at 15 kbar and 800–900 °C. Apatite is present at 10 kbar and 900 °C as well as 15 kbar and 800 °C and 1,000 °C. Titanite and allanite are present at 15 kbar and 800 °C.

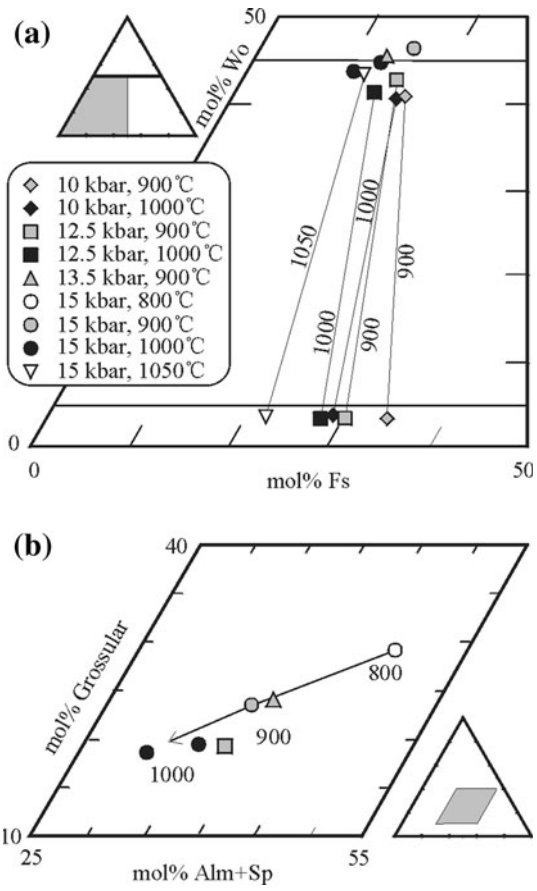

Fig. 4 **a** Compositions of pyroxenes projected into the pyroxene quadrilateral. **b** Compositions of garnets projected into the molar grossular-pyrope-almandine + spessartine triangle. Note that Mg/Fe of pyroxenes and pyrope proportion of garnet increase with temperature

Mineral compositions

Major elements of minerals are listed in Table 3. For zoned minerals, only the rim compositions are reported, which are considered to be in equilibrium with the partial melts.

Plagioclase has anorthite content ranging between An_{50} and An_{77}. Plagioclase crystals of the 10 kbar and 800 °C experiment contain the highest anorthite content (An_{77}) probably due to the high water content in the melt at these conditions.

Clinopyroxene crystals are mostly high-Ca augite and subordinately diopside, with a compositional range of $Wo_{40.9–46.5}En_{37.8–45.1}Fs_{10.8–17.3}$ (Fig. 4a). Clinopyroxene grains display some compositional zonings (Fig. 1h), with MgO and Al_2O_3 differences between the core and the rim reaching 0.1–1.7 and 0.3–2.2 wt%, respectively. Na and Al in clinopyroxene are 0.04–0.10 and 0.17–0.49 pfu (per formula unit), respectively, and show a general increase with pressure (Electronic Appendix 2). With the increase in temperature, Si decreases (Electronic Appendix 2) but Al increases indicating an increase in Ca-Tschermak ($CaAl_2SiO_6$) component, in agreement with Hermnan and Green (2001). TiO_2 and Mg# [Mg/(Mg + Fe)] of clinopyroxene are 0.7–1.5 wt% and 0.71–0.81, respectively, close to that

Table 4 Melt compositions normalized to 100 %, anhydrous totals

Run no.	C-3161	C-3179	C-3081	C-3180	C-3124	C-3136
P (kbar)	10	10	10	12.5	12.5	12.5
T (°)	800	900	1,000	800	900	1,000
n (major)	8	7	11	5	11	6
SiO_2	73.31 (0.65)	67.87 (0.65)	68.98 (1.26)	74.02 (0.12)	65.02 (0.34)	64.24 (0.40)
TiO_2	0.23 (0.05)	0.80 (0.04)	1.29 (0.08)	0.30 (0.03)	1.02 (0.06)	1.66 (0.05)
Al_2O_3	15.48 (0.17)	17.01 (0.23)	15.60 (0.56)	15.32 (0.14)	18.40 (0.21)	17.80 (0.27)
FeO^T	1.22 (0.07)	3.35 (0.34)	2.84 (0.26)	1.70 (0.07)	3.24 (0.26)	3.03 (0.22)
MnO	n.d.	0.03 (0.04)	0.05 (0.07)	0.07 (0.03)	0.01 (0.01)	0.01 (0.01)
MgO	0.60 (0.05)	1.25 (0.03)	1.42 (0.15)	0.53 (0.04)	1.74 (0.08)	2.31 (0.10)
CaO	4.05 (0.08)	4.52 (0.16)	4.25 (0.33)	2.86 (0.01)	5.39 (0.14)	5.79 (0.14)
Na_2O	3.80 (0.10)	3.12 (0.64)	3.19 (0.47)	2.84 (0.28)	3.59 (0.32)	3.54 (0.25)
K_2O	1.34 (0.04)	1.66 (0.09)	1.98 (0.08)	2.20 (0.04)	1.32 (0.06)	1.50 (0.08)
P_2O_5	n.d.	0.38 (0.07)	0.47 (0.08)	0.16 (0.03)	0.31 (0.13)	0.15 (0.05)
Hydrous total	85.18	90.21	90.17	89.18	91.07	92.12
H_2O (wt%)	20.8	13.0	13.8	19.4	9.2	6.1
Mg#	0.47	0.40	0.47	0.36	0.49	0.58
A/CNK	1.03	1.12	1.03	1.25	1.07	0.99
Qtz	35.68	31.15	31.90	41.62	24.35	21.68
Ab	32.11	26.36	26.95	24.00	30.32	29.90
An	20.10	20.20	18.30	13.26	24.92	27.85
Or	7.92	9.82	11.71	13.01	7.81	8.87
Cor	0.40	2.66	1.47	3.40	1.91	0.13
n (trace)	3	2	3	1	4	4
Li	63.9 (1.1)	65.4 (3.6)	42.8 (3.1)	93.9	50.2 (3.0)	44.9 (1.2)
Sc	5.59 (0.04)	6.07 (0.33)	22.7 (5.4)	3.79	7.03 (2.5)	13.3 (1.1)
Ti	589 (34)	4,518 (25)	6,610 (446)	1,703	5,625 (917)	8,854 (226)
V	16.9 (0.4)	14.6 (1.5)	38.3 (17.4)	3.75	10.4 (8.5)	23.7 (8.1)
Cr	n.d.	12.2	13.8 (7.9)	4.49	9.70	21.1 (11.6)
Rb	147 (1.5)	158 (6)	162 (21)	277	113 (1.7)	120 (6)
Sr	519 (4.0)	350 (13)	216 (7)	427	506 (31)	376 (24)
Y	11.0 (0.1)	18.0 (1.1)	23.3 (1.2)	7.39	11.0 (4.1)	21.3 (1.7)
Zr	190 (4.1)	148 (0)	111 (18)	121	180 (19.5)	137 (8)
Nb	106 (0.3)	249 (11)	73.4 (6.3)	263	146 (10.7)	131 (5)
Cs	149 (0.5)	153 (5)	205 (26)	271	119 (2.1)	115 (7)
Ba	2,086 (19)	1,226 (51)	1,029 (75)	1,952	1,287 (13)	1,126 (76)
La	100 (0.2)	73.3 (2.4)	52.9 (4.5)	68.6	84.25 (2.8)	52.8 (4.5)
Ce	117 (1.4)	113 (10)	90.8 (6.4)	94.5	135 (1.3)	85.5 (4.0)
Pr	48.8 (0.3)	56.4 (4.3)	49.0 (4.6)	40.2	70.0 (2.6)	46.2 (2.8)
Nd	39.2 (0.8)	56.4 (1.6)	53.1 (2.4)	32.3	66.6 (3.7)	48.5 (3.9)
Sm	24.0 (0.9)	40.9 (2.6)	49.5 (4.7)	18.3	50.6 (3.7)	41.7 (3.4)
Eu	25.0 (0.2)	40.7 (0.8)	29.6 (0.8)	29.0	48.3 (1.1)	41.6 (2.7)
Gd	17.9 (0.1)	33.7 (0.2)	46.0 (5.2)	13.4	33.7 (4.1)	40.2 (2.6)
Dy	17.9 (0.6)	32.8 (0.5)	44.5 (5.1)	11.5	22.4 (7.1)	39.4 (3.0)
Er	9.92 (0.25)	15.1 (0.1)	22.4 (0.9)	6.00	8.21 (3.7)	19.0 (1.2)
Yb	13.0 (0.2)	18.1 (0.3)	22.5 (0.2)	8.33	8.14 (4.2)	20.4 (1.4)
Lu	14.2 (0.1)	17.2 (0.2)	23.2 (1.3)	8.10	8.02 (4.1)	19.4 (1.4)
Hf	31.8 (1.7)	28.9 (1.0)	25.3 (4.6)	18.9	39.6 (4.5)	30.1 (1.2)
Ta	43.4 (0.4)	58.2 (1.6)	25.7 (2.1)	49.9	49.1 (5.1)	47.8 (2.0)
Pb	854 (7)	13.3 (1.7)	16.8 (4.6)	21.8	27.0 (3.9)	21.6 (2.5)

Table 4 continued

Run no.	C-3161	C-3179	C-3081	C-3180	C-3124	C-3136
Th	71.4 (0.8)	38.2 (1.8)	27.4 (3.1)	33.8	46.9 (3.0)	31.4 (2.0)
U	86.0 (0.7)	47.1 (5.2)	33.2 (3.3)	55.3	59.0 (1.7)	38.1 (0.8)
$(Sr/Y)_{SM}$	2.51	1.13	0.54	3.35	2.44	1.02
$(La/Yb)_{SM}$	3.49	1.92	1.11	3.90	4.67	1.23
$(Gd/Yb)_{SM}$	0.71	0.92	1.01	0.80	2.14	0.98
$(Eu/Eu^*)_{SM}$	1.13	1.07	0.61	1.81	1.10	0.99
$(Nb/Ta)_{SM}$	0.82	1.81	1.21	2.23	0.99	1.16
Run no.	C-3221	C-3171	C-3162	C-3052	C-3217	C-3123
P (kbar)	13.5	15	15	15	15	15
T (°)	900	800	900	1,000	1,000	1,050
n (major)	9	6	5	16	9	7
SiO_2	64.15 (0.67)	72.63 (0.44)	65.75 (0.92)	64.66 (1.09)	59.96 (0.25)	57.91 (0.35)
TiO_2	0.96 (0.07)	0.32 (0.03)	0.85 (0.07)	1.15 (0.11)	1.47 (0.10)	1.44 (0.10)
Al_2O_3	18.61 (0.19)	16.17 (0.09)	18.1 (0.2)	17.63 (1.06)	18.93 (0.14)	19.90 (0.15)
FeO^T	3.80 (0.11)	1.77 (0.14)	3.40 (0.13)	3.36 (0.25)	4.88 (0.14)	5.36 (0.15)
MnO	0.02 (0.05)	0.02 (0.08)	0.03 (0.04)	0.02 (0.03)	0.01 (0.02)	0.03 (0.05)
MgO	1.95 (0.08)	0.60 (0.03)	1.47 (0.05)	1.53 (0.12)	3.20 (0.05)	3.55 (0.22)
CaO	6.42 (0.09)	4.61 (0.07)	5.49 (0.15)	5.34 (0.53)	7.04 (0.09)	7.80 (0.24)
Na_2O	2.77 (0.20)	2.59 (0.32)	3.44 (0.12)	4.02 (0.34)	3.24 (0.31)	3.10 (0.13)
K_2O	0.97 (0.03)	1.13 (0.03)	1.09 (0.04)	1.26 (0.12)	0.93 (0.04)	0.85 (0.02)
P_2O_5	0.40 (0.06)	0.16 (0.05)	0.41 (0.05)	0.68 (0.15)	0.35 (0.04)	0.09 (0.05)
Hydrous total	85.15	88.22	87.59	92.25	89.51	92.53
H_2O (wt%)	8.3	10.2	14.5	3.4	3.4	2.9
Mg#	0.48	0.38	0.44	0.45	0.54	0.54
A/CNK	1.08	1.16	1.07	1.00	0.99	0.98
Qtz	26.87	41.94	27.03	23.20	16.45	12.45
Ab	23.39	21.89	29.07	34.09	27.37	26.18
An	29.50	21.94	24.84	22.59	32.87	37.80
Or	5.73	6.68	6.45	7.48	5.50	5.02
Cor	2.17	2.63	2.10	1.39	0.52	0.00
n (trace)	8	6	7	11	10	6
Li	47.6 (0.9)	60.7 (1.9)	44.5 (1.2)	43.0 (1.7)	41.3 (0.6)	34.4 (0.7)
Sc	5.10 (0.30)	4.94 (2.64)	11.1 (3.7)	8.88 (3.11)	7.37 (0.35)	16.1 (1.3)
Ti	4,745 (106)	1,875 (724)	4,327 (217)	6,497 (237)	7,389 (100)	7,467 (328)
V	7.56 (1.21)	3.05 (4.77)	26.0 (8.7)	28.7 (15.7)	14.9 (1.2)	19.5 (3.9)
Cr	n.d.	6.8	9.5 (3.6)	20.3	n.d.	4.7 (1.2)
Rb	96.5 (2)	137 (7)	92.7 (6)	101 (8)	79.0 (0.7)	70.2 (1.2)
Sr	552 (12)	556 (23)	552 (39)	569 (34)	504 (5)	459 (12)
Y	2.89 (0.18)	9.45 (2.34)	4.28 (0.76)	4.41 (0.88)	7.57 (0.23)	23.7 (0.9)
Zr	123 (5)	130 (8)	109 (6)	109 (9)	112 (2)	126 (5)
Nb	132 (5)	115 (4)	131 (8)	152 (15)	118 (1)	109 (4)
Cs	94.2 (1.2)	139 (6)	90.3 (6.2)	125 (15)	77.2 (0.8)	67.5 (1.7)
Ba	1,090 (32)	1,484 (69)	1,082 (61)	1,273 (110)	989 (11)	892 (28)
La	69.8 (2.4)	70.3 (5.1)	71.3 (4.6)	81.9 (6.1)	61.6 (1.2)	57.5 (2.3)
Ce	109 (5)	97.7 (4.8)	113 (6)	130 (10)	103 (1)	94.6 (3.8)
Pr	58.0 (1.9)	43.9 (1.4)	59.6 (2.2)	69.0 (6.0)	55.2 (0.8)	52.1 (2.2)
Nd	56.3 (2.5)	37.7 (1.2)	56.8 (2.1)	66.6 (7.1)	57.3 (0.9)	52.6 (2.3)
Sm	38.7 (1.5)	24.4 (2.8)	35.9 (2.1)	45.9 (4.1)	46.6 (1.2)	47.4 (2.3)

Table 4 continued

Run no.	C-3221	C-3171	C-3162	C-3052	C-3217	C-3123
Eu	39.5 (0.9)	28.9 (1.5)	34.5 (0.5)	45.3 (2.7)	47.5 (0.7)	49.4 (2.0)
Gd	21.8 (0.8)	18.3 (3.7)	19.4 (1.0)	25.1 (3.9)	33.3 (0.9)	42.7 (2.4)
Dy	8.13 (0.31)	16.5 (4.6)	10.6 (1.6)	11.2 (1.7)	19.0 (0.7)	41.3 (2.1)
Er	1.89 (0.14)	8.20 (2.21)	3.38 (0.78)	3.51 (1.08)	5.25 (0.21)	20.1 (1.0)
Yb	1.14 (0.15)	10.1 (2.1)	2.67 (0.67)	2.22 (0.73)	3.51 (0.20)	20.8 (0.8)
Lu	0.94 (0.10)	10.7 (2.1)	2.80 (0.80)	1.97 (0.65)	2.79 (0.14)	20.5 (0.9)
Hf	30.7 (1.1)	24.8 (2.1)	27.9 (1.8)	30.0 (2.0)	28.9 (0.5)	28.0 (0.9)
Ta	45.2 (2.4)	40.0 (1.7)	46.3 (3.0)	53.6 (6.5)	41.8 (1.1)	38.2 (1.3)
Pb	35.7 (0.6)	37.6 (1.8)	121 (7)	59.8 (9.4)	35.9 (1.5)	28.4 (1.7)
Th	34.1 (2.0)	42.5 (3.8)	36.1 (2.7)	41.3 (3.2)	30.0 (0.6)	26.8 (1.3)
U	80.3 (2.6)	56.6 (3.5)	44.8 (2.6)	45.8 (3.9)	36.9 (0.7)	34.3 (1.1)
$(Sr/Y)_{SM}$	11.1	3.41	9.46	7.48	3.86	1.12
$(La/Yb)_{SM}$	29.1	3.29	17.1	17.5	8.32	1.31
$(Gd/Yb)_{SM}$	9.48	0.89	4.47	5.61	4.70	1.02
$(Eu/Eu^*)_{SM}$	1.33	1.34	1.29	1.30	1.18	1.07
$(Nb/Ta)_{SM}$	1.23	1.21	1.19	1.20	1.19	1.21

Units in parentheses are standard deviations (1σ) of multiple analyses. *n.d.* not detected. SM, normalization to the starting material. $(Eu/Eu^*)_{SM} = Eu_{SM}/(Sm_{SM} \times Gd_{SM})^{0.5}$. Qtz, Ab, An and Cor are CIPW normative quartz, albite, anorthite and corundum, respectively. H_2O in melt was estimated by assuming that all added water is hosted in melt and amphibole and no water was lost during the capsule welding

obtained in former experiments (Sen and Dunn 1994; Rapp and Watson 1995; Grove et al. 1997; Springer and Seck 1997; Xiong et al. 2005, 2009).

Orthopyroxene crystals have a compositional range of $Wo_{3.4–3.9}En_{62.1–73.9}Fs_{22.2–34.3}$ (Fig. 4a). They show some compositional zoning (Fig. 1e), with Al_2O_3 and MgO differences between the core and the rim reaching 0.3–1.4 and 0.1–1.6 wt%, respectively. Al pfu in orthopyroxene increases with temperature and also pressure (Electronic Appendix 2b). Mg# (0.65–0.77) of orthopyroxene is positively correlated with temperature and the degree of melting. TiO_2 content ranges about 0.36–0.57.

Amphibole crystals are homogeneous in composition. They belong to magnesiohornblende in the 10 kbar and 800 °C experiment and tschermakite in the other runs. TiO_2 (1.7–3.5 wt%) in amphibole is close to that of Sen and Dunn (1994) and Springer and Seck (1997). Al_2O_3 (13.2–16.2 wt%) in amphibole increases with pressure and temperature. Mg# of amphibole is 0.57–0.68, exhibiting an increase with temperature.

Garnet crystals are homogeneous in major elements. Grossular, almandine, and pyrope fractions are 18–28, 31–47, and 24–50 %, respectively. Pyrope increases but grossular and almandine decrease with increasing temperature (Fig. 4b), in agreement with the other experiments (Sen and Dunn 1994; Rapp and Watson 1995; Springer and Seck 1997).

Melt compositions

Major and trace elements of the quenched melts are listed in Table 4. The partial melts are homogeneous in composition, as relative standard deviations are <10 % for most of the elements except P, Mn, V, and Cr. The partial melts have anhydrous silica contents ranging between 57.9 and

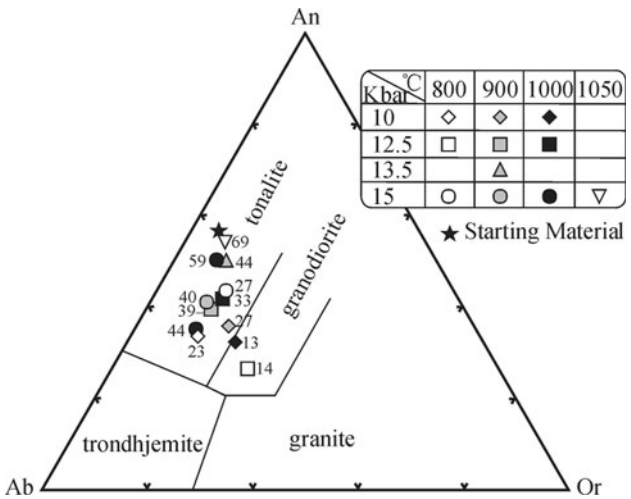

Fig. 5 Normative albite (Ab)- anorthite (An)- orthoclase (Or) plot for the partial melts. Data beside symbols represent melt proportions (wt%) estimated by mass balance

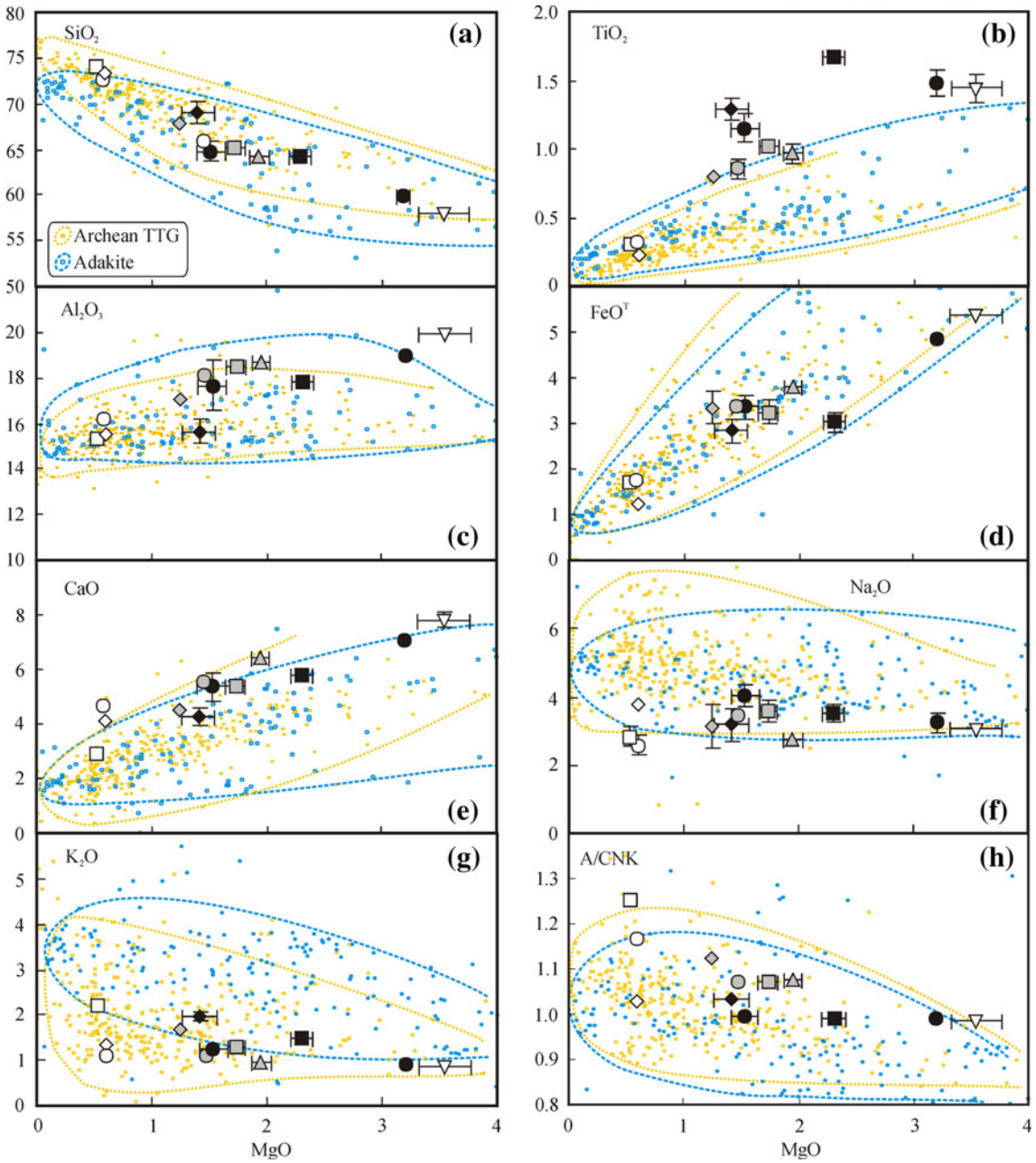

Fig. 6 Plots of SiO_2 (**a**), TiO_2 (**b**), Al_2O_3 (**c**), FeO^T (**d**), CaO (**e**), Na_2O (**f**), K_2O (**g**) and A/CNK (**h**) versus MgO for the partial melts. Symbols for the partial melts are the same as in Fig. 5. 316 Archean TTG (Martin 1987; Sage et al. 1996; Liu et al. 2004; Condie 2005; Clemens et al. 2006; Diwu et al. 2007; Moyen et al. 2007; Jahn et al. 2008; Turkina et al. 2009; Huang et al. 2010) and 204 adakitic rocks from North China and South China (Gao et al. 2004; Wang et al. 2006; Xu et al. 2002, 2006; Jiang et al. 2007; Qian and Hermann 2010), Tibet plateau (Chung et al. 2003; Hou et al. 2004; Guo et al. 2007) and circum-Pacific arcs (Atherton and Petford 1993; Muir et al. 1995; Petford and Atherton 1996) are shown for comparison

74.0 wt% and vary from granodiorite to tonalite with increasing degree of melting (Fig. 5). The amount of CIPW normative quartz is between 13 and 46 wt%. Normative corundum is zero at 15 kbar and 1,050 °C and between 0.1 and 4.4 wt% in the other experiments. Mg# varies between 0.36 and 0.58, and anhydrous MgO, Al_2O_3, and TiO_2 of the quenched melts are 0.5–3.6, 15.3–19.9, and 0.2–1.7 wt%, respectively. In the Harker diagrams (Fig. 6), SiO_2, TiO_2, Al_2O_3, FeO^T, and CaO of the partial melts display a linear correlation with MgO. It is notoriously difficult to analyze Na_2O in hydrous silicate glass. We have used scans of melt pools to minimize loss of Na during analysis. Nevertheless, mass balance calculation indicates that Na loss was 15–30 % in the 13.5 kbar and 900 °C and 15 kbar and

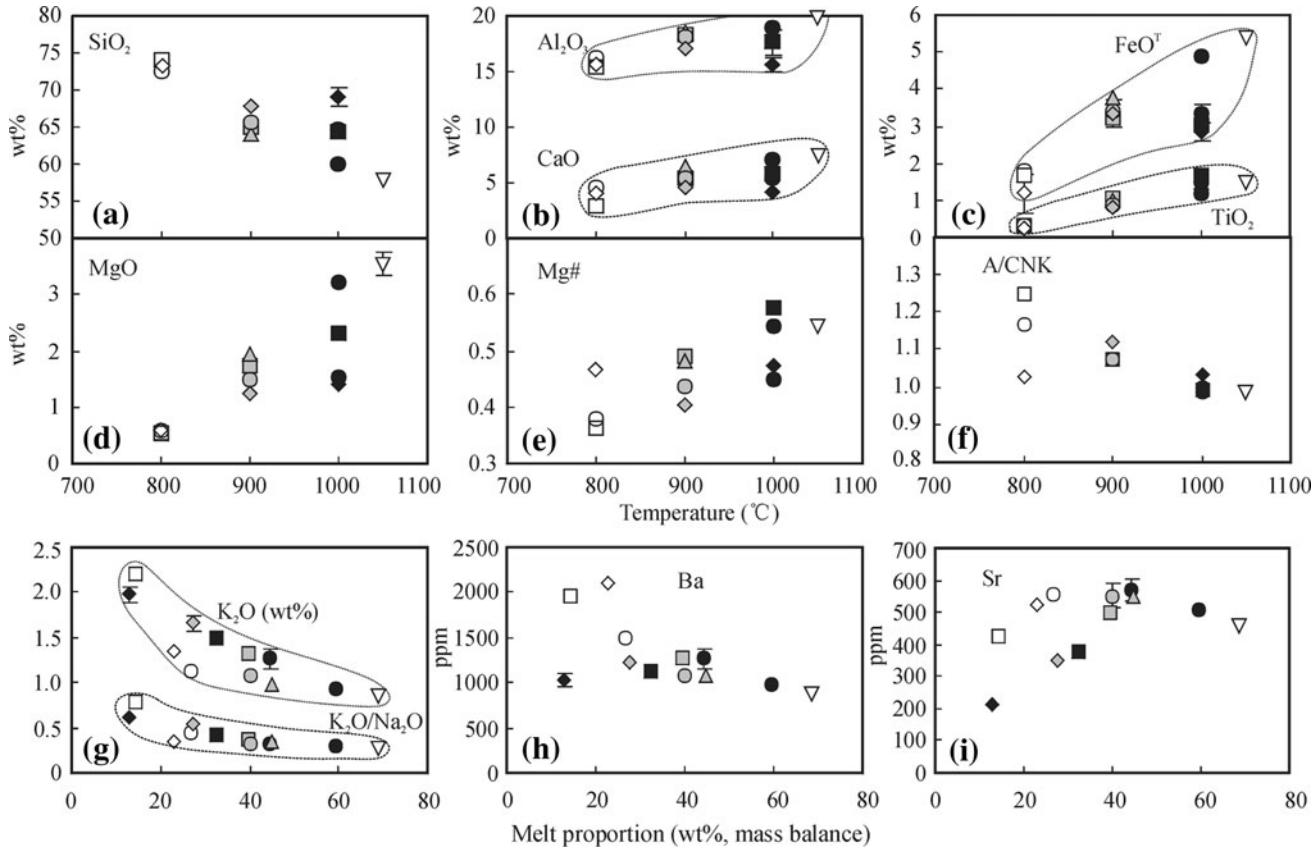

Fig. 7 Plots of SiO_2 (**a**), Al_2O_3 and CaO (**b**), FeO^T and TiO_2 (**c**), MgO (**d**), Mg# (**e**) and A/CNK (**f**) versus temperature, and K_2O and K_2O/Na_2O (**g**), Ba (**h**) and Sr (**i**) versus melt proportion (by mass balance) for the partial melts. *Symbols* are the same as in Fig. 5. *Error bars* refer to 1 standard deviation from multiple analyses and are smaller than the size of the symbol when not shown. It is notable in (**i**) that Sr in the melt is controlled by residual plagioclase at low to moderate degrees of melting of amphibolite and granulite and is diluted when plagioclase disappears at high melting degrees

900–1,000 °C experiments and <10 % in the other runs. Thus, Na loss may not have significantly affected the melt compositions.

Al_2O_3, CaO, FeO^T, TiO_2, MgO, and Mg# of the partial melts show a general increase with temperature and melt proportion, in agreement with Winther (1996), whereas SiO_2, K_2O, and A/CNK [molar $Al_2O_3/(CaO + Na_2O + K_2O)$] (1.25–0.98) decrease (Fig. 7). The partial melts change from peraluminous to slightly metaluminous with increasing melting. K_2O/Na_2O decreases rapidly from 0.8 to 0.4–0.3 as melting degree increases from 15 to 40 wt% and approaches the value (0.2) of the starting material with further melting (Electronic Appendix 3). Strontium increases first with melting and reaches a climax as the residual plagioclase is consumed (at ~40 wt% melting) and then decreases with further melting (Fig. 7i). Highly incompatible elements such as Cs, Rb, and Ba are inversely correlated with melt proportions.

Al_2O_3, Sr, Gd, Dy, Yb, Sr/Y, Gd/Yb, and La/Yb of the partial melts vary with pressure and are sensitive to the proportions of residual plagioclase, amphibole, and/or garnet (Fig. 8). Al_2O_3 and Sr increase with pressure and with decreasing amount of plagioclase. Gd, Dy, and Yb are depressed, and Gd/Yb and La/Yb are strongly elevated in melts coexisting with high proportions of amphibole and especially garnet. Sr/Y is also conspicuously elevated when residual garnet and amphibole are high (Fig. 8f).

Highly incompatible elements (Cs to Pr) of the melts vary by a factor of less than 4, while HREE vary by a factor of up to 20. The trace elements contents of melts have been normalized to the starting composition in order to highlight fractionation trends during partial melting (Fig. 9). Melts at 10–12.5 kbar and 1,000 °C and 15 kbar and 1,050 °C have flat REE patterns, with elevated HREE relative to the starting material. Melts at 13.5 kbar and 900 °C and 15 kbar and 900–1,000 °C are strongly depleted in HREE, whereas melts at 10–15 kbar and 800 °C are moderately depleted in middle and HREE. In addition, melts at 800 °C show uphill patterns from Gd to Lu. The normalized patterns at 10 kbar and 1,000 °C have strong Sr and Eu depletions. Ti is depleted relative to the starting material in the 800–900 °C melts. The 10 kbar and 800 °C melts have

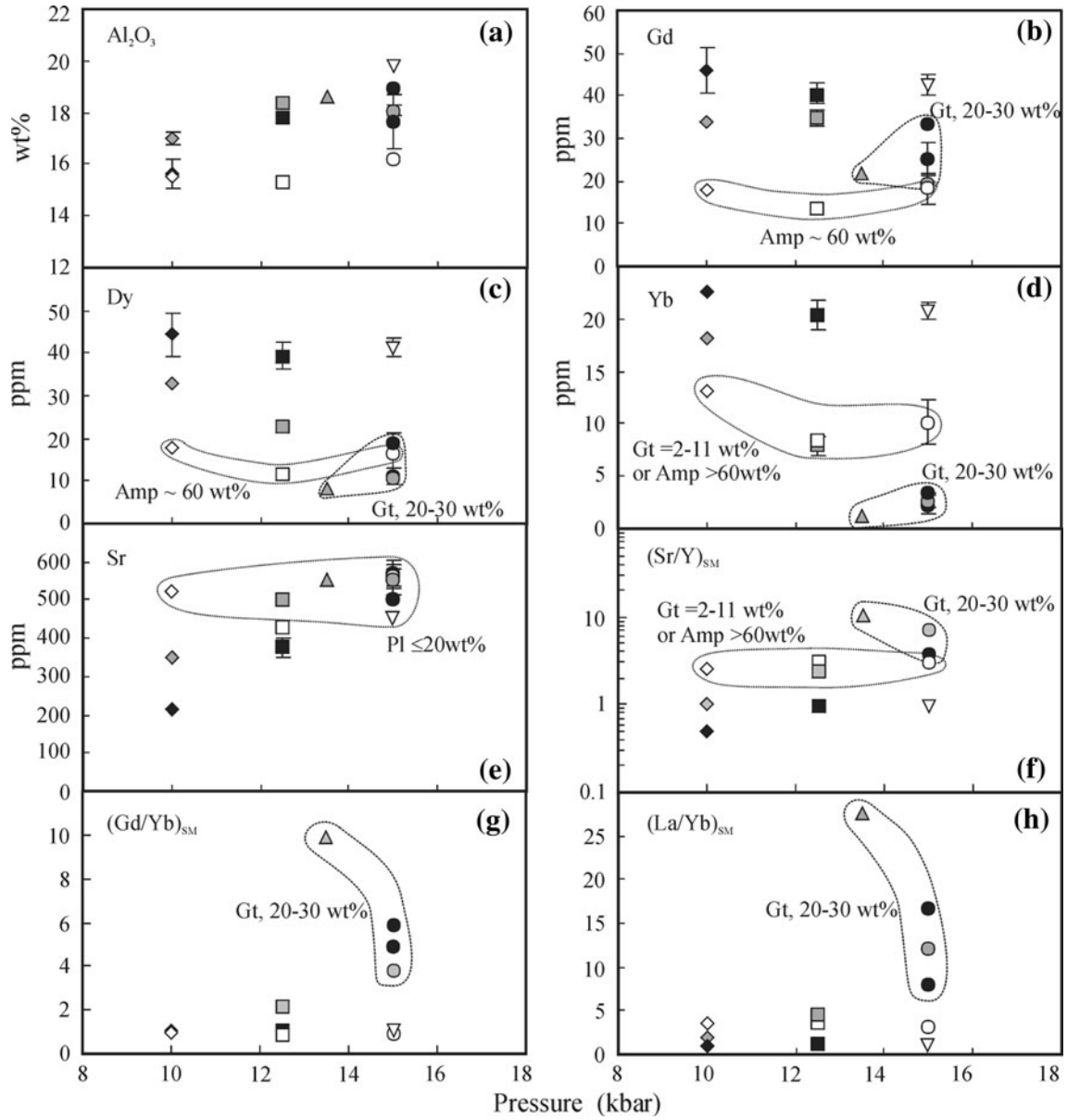

Fig. 8 Plots of Al_2O_3 (**a**), Gd (**b**), Dy (**c**), Yb (**d**), Sr (**e**), $(Sr/Y)_{SM}$ (**f**), $(Gd/Yb)_{SM}$ (**g**) and $(La/Yb)_{SM}$ (**h**) versus pressure for the partial melts. *Symbols* are the same as in Fig. 5. SM indicates normalization by the starting material

a small Nb–Ta trough (Fig. 9a) probably due to high amounts of coexisting ilmenites. Zr and Hf are enriched to various degrees in all the melts.

Mineral/melt trace element partitioning

Trace element analyses made by LA-ICP-MS for plagioclase, amphibole, garnet, and orthopyroxene are listed in Table 5. Clinopyroxene and accessory minerals were not analyzed for trace elements due to the small size (<20 μm). The Nernst partition coefficients (D) between minerals and melts were calculated using the equation

$$D_i^{\text{mineral/melt}} = C_i^{\text{mineral}} / C_i^{\text{melt}} \quad (1)$$

in which C_i^{mineral} and C_i^{melt} represent the concentrations of element i in the mineral and melt, respectively. The experimental partition coefficients are mostly close to that formerly determined in andesitic, dacitic, or rhyolitic melts under similar temperatures (Table 6; Fig. 10). $D_{\text{Eu}}^{\text{pl/melt}}$ (1.04–1.42) is in good agreement with that predicted by the experimental $D_{\text{Eu}}^{\text{pl/melt}}$-$f_{O_2}$ relationship of Wilke and Behrens (1999) at Δ(QFM) of −2, despite the difference in plagioclase and melt compositions. $D_{\text{La}}^{\text{pl/melt}}$ values are similar to that of Severs et al. (2009), while $D^{\text{pl/melt}}$ values

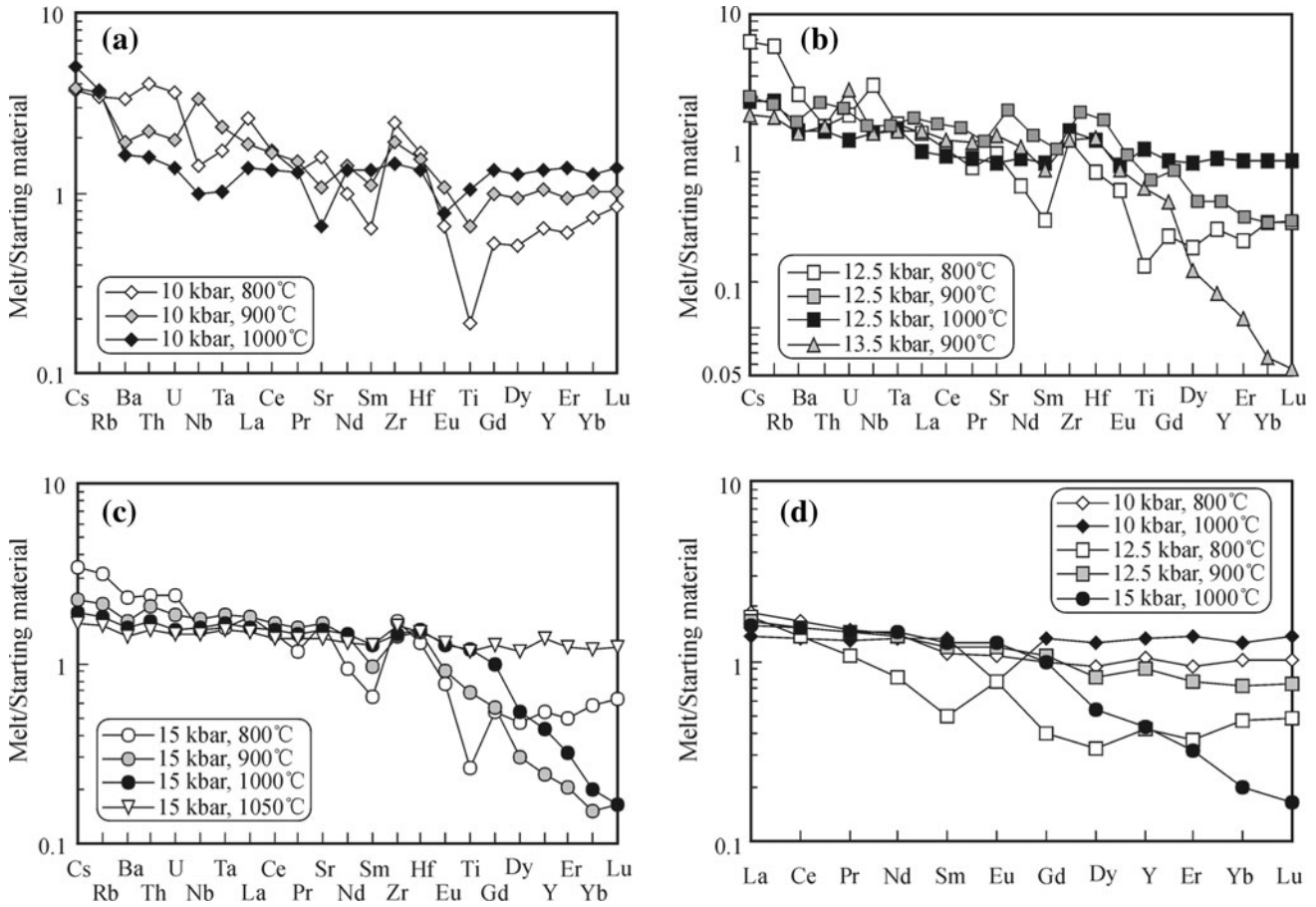

Fig. 9 Incompatible trace elements of the partial melts normalized by the starting material

for the middle and heavy REE are 3–10 times higher (Fig. 10a), indicating some (~10 %) melt contamination in our analysis. Middle and heavy REE are compatible in amphibole, with maximum $D_{REE}^{amph/melt}$ at Er (Electronic Appendix 4a). $D_{Nb}^{amph/melt}/D_{Ta}^{amph/melt}$ and $D_{Zr}^{amph/melt}/D_{Sm}^{amph/melt}$ are 1.4 and 0.2, respectively, close to that determined by Foley et al. (2002) and Nehring et al. (2010) for low-magnesium amphibole. $D_{Zr}^{amph/melt}/D_{Hf}^{amph/melt}$ is 0.60, similar to the value (0.58 ± 0.06) reported by Tiepolo et al. (2007). $D_{REE}^{gt/melt}$ values obtained at 12.5 kbar and 900 °C and at 15 kbar and 900–1,000 °C ($D_{La}^{gt/melt}$ = 0.005–0.025, $D_{Yb}^{gt/melt}$ = 11.7–34.8) are similar to that determined in former experiments (Arth 1976; Klein et al. 2000; Koepke et al. 2003; Klemme et al. 2002). However, $D_{Yb}^{gt/melt}$ values obtained at 13.5 kbar and 900 °C (189 ± 94) are much higher and also highly variable. The garnets in this experiment are smaller (Fig. 1f), and thus, it was not possible to obtain clean rim compositions of garnets. As garnet display high HREE in the core, the $D_{Yb}^{gt/melt}$ in this experiment is likely overestimated. $D_{Nb}^{gt/melt}/D_{Ta}^{gt/melt}$, $D_{Zr}^{gt/melt}/D_{Hf}^{gt/melt}$, and $D_{Ti}^{gt/melt}/D_{Zr}^{gt/melt}$ are 0.34–0.86, 1.65–1.98, and 1.04–1.86, respectively, and $D_{Ti}^{gt/melt}$ and $D_{Ti}^{gt/melt}/D_{Zr}^{gt/melt}$ are positively correlated with mole% Ca (0.18–0.24) in garnets. The experimental garnets have $D_{Ti}^{gt/melt} > D_{Zr}^{gt/melt} > D_{Hf}^{gt/melt}$, in agreement with van Westrenen et al. (2001). For all the experimental amphibole, garnet, and orthopyroxene, a negative anomaly of D_{Eu} is observed (Fig. 10). This is likely related to the fact that some Eu are present in a divalent state under the experimental conditions. In the Onuma diagrams, $D_{REE}^{amph/melt}$, $D_{REE}^{gt/melt}$, and $D_{REE}^{opx/melt}$ display parabolic curves as predicted by the lattice strain model (Blundy and Wood 1994) (Electronic Appendix 4).

Bulk partitioning of trace elements

Bulk partition coefficients (D_i^{bulk}) of trace elements between the residue and melt were estimated using two methods. First, D_i^{bulk} was calculated by the following expression

$$D_i^{bulk} = \left(C_i^{SM} - F \times C_i^{melt}\right)/\left(C_i^{melt} - F \times C_i^{melt}\right) \quad (2)$$

where F is the actual melt proportion in weight percent (Table 2), and C_i^{SM} and C_i^{melt} are the concentrations of a

Table 5 Trace elements of minerals analyzed with LA-ICP-MS

Mineral	Pl	Pl	Amp	Gt	Gt	Gt	Gt	Gt	Opx
Run no.	C-3180	C-3136	C-3124	C-3124	C-3221	C-3162	C-3052	C-3217	C-3179
P (kbar)	12.5	12.5	12.5	12.5	13.5	15	15	15	10
T (°)	800	1,000	900	900	900	900	1,000	1,000	900
n	1	2	5	5	7	4	16	4	3
Li	18.8	11.3 (0.1)	7.27 (0.44)	4.58 (0.57)	4.33 (0.26)	6.18 (0.39)	8.24 (1.07)	2.78 (0.74)	12.0 (0.7)
Sc	2.13	2.78 (0.33)	39.4 (1.9)	62.0 (9.4)	81.2 (16.4)	56.0 (1.8)	54.3 (12.9)	82.1 (10.0)	39.6 (5.0)
Ti	389	1,122 (128)	17,400 (1,093)	6,877 (479)	6,263 (279)	6,399 (409)	8,119 (1,573)	2,700 (521)	2,641 (500)
V	4.8	7.20 (2.35)	136 (16)	84.6 (7.5)	83.7 (12.8)	74.7 (2.3)	78.8 (4.2)	96.7 (16.6)	119.2 (26.8)
Cr	bdl	bdl	39.3 (10.1)	27.6 (2.9)	36.4 (12.3)	22.0 (2.2)	32.2 (6.6)	60.0 (24.6)	39.2 (10.9)
Rb	0.54	12.7 (2.3)	5.14 (0.91)	bdl	0.85 (0.05)	bdl	bdl	2.78 (0.78)	1.13 (1.03)
Sr	966	632 (72)	181 (22)	2.39 (1.42)	6.54 (3.09)	2.24 (1.42)	1.17 (0.86)	13.2 (7.4)	18.2 (5.3)
Y	0.946	2.29 (0.35)	34.7 (2.4)	105 (34)	137 (39)	62.5 (8.4)	71.2 (35.4)	83.5 (12.0)	7.0 (0.7)
Zr	1.65	13.9 (3.8)	33.6 (3.0)	119 (22)	90.8 (4.2)	111 (13)	117 (26)	39.3 (10.6)	10.7 (0.6)
Nb	2.15	12.5 (3.0)	49.5 (4.5)	2.12 (0.58)	4.85 (1.10)	5.34 (1.50)	4.34 (2.23)	4.66 (2.93)	6.55 (1.88)
Cs	bdl	11.1 (2.4)	0.514 (0.196)	bdl	bdl	bdl	bdl	1.92 (1.24)	1.15 (1.25)
Ba	177	275 (9)	185 (11)	2.24 (0.23)	4.75 (2.82)	bdl	1.12 (0.42)	24.8 (15.9)	19.9 (7.2)
La	8.55	16.0 (11.7)	7.49 (0.34)	0.462 (0.277)	0.527 (0.174)	0.371 (0.184)	0.370 (0.183)	1.56 (0.98)	1.58 (0.32)
Ce	10.3	13.3 (1.6)	24.7 (1.8)	1.92 (0.71)	1.91 (0.53)	1.84 (0.35)	1.84 (0.52)	3.15 (1.52)	3.75 (0.37)
Pr	4.52	6.56 (1.01)	22.2 (2.1)	3.02 (0.65)	2.95 (0.53)	3.24 (0.32)	3.19 (0.73)	2.37 (0.94)	2.86 (0.49)
Nd	3.82	6.38 (1.29)	34.3 (3.1)	9.13 (0.63)	8.40 (1.03)	9.62 (1.00)	10.0 (2.1)	4.34 (0.87)	4.30 (1.36)
Sm	2.45	5.67 (0.74)	48.9 (4.2)	43.6 (3.5)	40.3 (2.2)	41.5 (4.8)	42.9 (9.7)	19.1 (4.1)	5.88 (1.47)
Eu	41.2	43.4 (1.6)	39.2 (0.9)	43.3 (2.7)	49.5 (2.0)	57.9 (6.6)	42.2 (7.0)	21.9 (2.9)	4.62 (1.21)
Gd	2.04	4.55 (0.42)	57.9 (3.9)	106 (15)	101 (8)	81.3 (10.6)	90.3 (26.7)	58.1 (15.0)	7.99 (2.00)
Dy	1.89	4.20 (1.03)	63.9 (4.2)	172 (44)	215 (48)	112 (16)	129 (56)	128 (22)	11.7 (1.7)
Er	0.941	1.91 (0.48)	31.4 (3.1)	92.6 (34.4)	157 (55)	64.2 (9.5)	71.8 (38.2)	91.8 (12.6)	7.36 (0.71)
Yb	0.728	2.23 (0.27)	30.8 (2.9)	95.2 (38)	215 (94)	70.4 (11.8)	77.4 (45.9)	112 (17)	11.1 (0.8)
Lu	0.748	1.92 (0.35)	27.5 (3.1)	89.2 (35.8)	229 (107)	70.7 (12.5)	77.0 (45.9)	116 (19)	11.1 (0.1)
Hf	0.688	2.30 (0.14)	12.3 (1.1)	15.2 (0.9)	11.4 (0.7)	15.3 (2.0)	18.2 (4.0)	6.1 (1.5)	4.13 (0.41)
Ta	0.380	3.88 (0.47)	11.8 (0.6)	2.14 (0.44)	3.53 (0.47)	3.67 (0.71)	3.81 (1.58)	1.92 (1.08)	1.61 (0.28)
Pb	16.0	9.09 (6.67)	2.59 (1.14)	bdl	0.441 (0.117)	bdl	bdl	0.963 (0.529)	0.793 (0.350)
Th	bdl	2.75 (0.37)	0.539 (0.034)	bdl	0.312 (0.077)	bdl	0.430 (0.216)	0.739 (0.448)	0.559 (0.129)
U	0.091	3.49 (0.76)	0.907 (0.123)	1.72 (0.22)	3.24 (0.53)	1.97 (0.50)	2.29 (0.95)	1.39 (0.54)	0.652 (0.441)

Numbers in parentheses refer to standard deviations (1σ) of multiple analyses. *bdl* below detection limit

specific element i in starting material (Table 1) and partial melt (Table 4), respectively. Bulk partition coefficients determined by this method are reported in Electronic Appendix 5a.

Alternatively, D_i^{bulk} was calculated by

$$D_i^{\text{bulk}} = x_1 D_1^{\text{mineral/melt}} + x_2 D_2^{\text{mineral/melt}} + x_3 D_3^{\text{mineral/melt}} \cdots \quad (3)$$

where x_1 is the percentage proportion of mineral 1 in the residue and $D_1^{\text{mineral/melt}}$ is the partitioning of trace element i between mineral 1 and melt. This approach has the advantage that the trace element pattern of small melt fractions, which is difficult to produce in experiments, can be assessed. In this approach, the proportions of minerals (x_i) at a given melting degree (e.g., 5, 10, or 20 wt%) were estimated by mass balance, in which the experimental mineral and melt compositions were used. Alternatively, an average of 144 adakitic rocks (Atherton and Petford 1993; Muir et al. 1995; Petford and Atherton 1996; Chung et al. 2003; Gao et al. 2004; Hou et al. 2004; Wang et al. 2006; Xu et al. 2002, 2006; Guo et al. 2007; Jiang et al. 2007; Qian and Hermann 2010) with <3.0 wt% MgO was used to

Table 6 Mineral/melt partition coefficients

Mineral	Pl	Pl	Amp	Gt	Gt	Gt	Gt	Gt	Opx	Pl	Amp	Gt	Opx
Run no.	C-3180	C-3136	C-3124	C-3124	C-3221	C-3162	C-3052	C-3217	C-3179	Literature			
P (kbar)	12.5	12.5	12.5	12.5	13.5	15	15	15	10				
T (°)	800	1,000	900	900	900	900	1,000	1,000	900				
Li	0.200	0.252	0.145	0.091	0.091	0.139	0.192	0.067	0.197				
Sc	0.563	0.210	5.609	8.828	15.921	5.070	6.114	11.136	8.022	0.053	35.0		
Ti	0.228	0.127	3.094	1.223	1.320	1.479	1.250	0.365	1.409	0.043	2.020–13.190	0.210–2.620	
V	1.282	0.304	13.066	8.131	11.065	2.870	2.740	6.511	39.125		4.920		
Cr	–	–	4.054	2.848	–	2.314	1.586	–	5.773		21.0		
Rb	0.002	0.106	0.045	–	0.009	–	–	0.035	0.008	0.048–0.105	0.14	0.001–0.009	0.003–0.022
Sr	2.262	1.679	0.358	0.005	0.012	0.004	0.002	0.026	0.033	2.422–15.633	0.280–0.490	0.005–0.126	0.009–0.032
Y	0.128	0.107	3.156	9.532	47.266	14.608	16.141	11.028	0.743	0.012–0.130	1.300–3.100	2.90–39.00	1.000
Zr	0.014	0.102	0.187	0.656	0.740	1.012	1.069	0.352	0.082	0.005–0.135	0.230–1.060	0.40–2.20	0.200
Nb	0.008	0.095	0.339	0.015	0.037	0.041	0.029	0.040	0.057	0.008	0.200–1.000	0.008–0.080	0.800
Cs	–	0.097	0.004	–	0.008	–	0.002	0.025	0.008	0.105			
Ba	0.091	0.244	0.144	0.002	0.004	–	0.001	0.025	0.013	0.186–1.515	0.120	0.00004–0.017	0.003–0.013
La	0.125	0.303	0.089	0.005	0.008	0.005	0.005	0.025	0.022	0.088–0.380	0.100–0.640	0.0006–0.066	
Ce	0.109	0.156	0.184	0.014	0.018	0.016	0.014	0.030	0.038	0.240–0.267	0.220–0.630	0.0034–0.350	0.030–0.150
Pr	0.112	0.142	0.317	0.043	0.051	0.054	0.046	0.043	0.065				
Nd	0.118	0.132	0.514	0.137	0.149	0.169	0.151	0.076	0.114	0.054–0.203	0.620–1.240)	0.13–4.50	0.047–0.220
Sm	0.134	0.136	0.966	0.862	1.042	1.155	0.935	0.410	0.241	0.013–0.165	0.660–3.580	0.17–15.0	0.082–0.270
Eu	1.421	1.042	0.811	0.896	1.256	1.678	0.933	0.462	0.160	0.397–5.417	1.080	1.10–9.80	0.069–0.170
Gd	0.152	0.113	1.718	3.149	4.662	4.178	3.590	1.744	0.437	0.037–0.125	1.490–4.000	0.59–29.0	0.132–0.340
Dy	0.163	0.107	2.859	7.701	26.395	10.525	11.537	6.716	0.708	0.013–0.112	1.770–3.080	7.30–36.0	0.212–0.460
Er	0.157	0.101	3.825	11.282	82.989	19.005	20.484	17.478	0.897	0.084	1.470–2.340	9.30–42.8	0.314–0.650
Yb	0.087	0.109	3.786	11.697	188.973	26.327	34.833	32.015	1.097	0.010–0.090	1.150–1.310	10.0–52.5	0.438–0.860
Lu	0.092	0.099	3.426	11.129	242.483	25.278	39.111	41.527	1.031	0.062–0.092	0.980–2.520	7.90–76.0	0.646–0.900
Hf	0.036	0.077	0.311	0.384	0.373	0.547	0.606	0.213	0.166	0.016–0.148	0.430–1.870	0.31–1.30	
Ta	0.008	0.081	0.239	0.044	0.078	0.079	0.071	0.046	0.040	0.035	0.170–1.600	0.004–0.080	
Pb	0.733	0.421	0.096	–	0.012	–	–	0.027	0.021	0.134–0.972			
Th	–	0.088	0.011	–	0.009	–	0.010	0.025	0.013	0.048	0.017	0.0015–0.3400	
U	0.002	0.092	0.015	0.029	0.040	0.044	0.050	0.038	0.012	0.093	0.008	0.006–0.850	

Literature partition coefficients for plagioclase (Arth 1976; Nath and Crecraft 1985; Severs et al. 2009), amphibole (Sisson 1994; Brenan et al. 1995; Klein et al. 1997; Hilyard et al. 2000), garnet (Arth 1976; Klein et al. 2000; Klemme et al. 2002; Koepke et al. 2003; Rubatto and Hermann 2007) and orthopyroxene (Arth 1976; Philpotts and Schnetzler 1970; Schnetzler and Philpotts 1970) in andesitic–rhyolitic melts are cited for comparison. –, not obtained

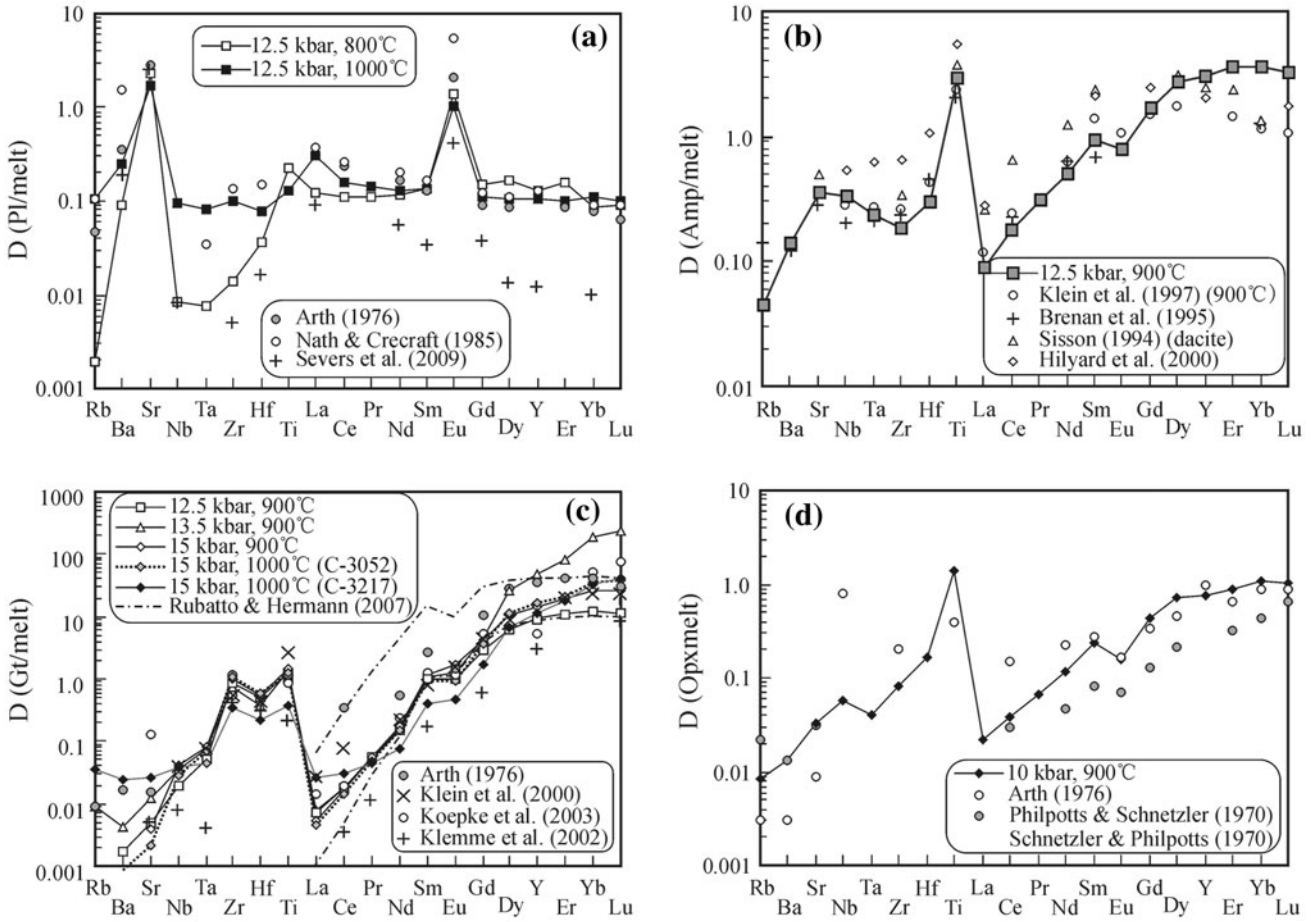

Fig. 10 Mineral-melt partition coefficients for plagioclase (**a**), amphibole (**b**), garnet (**c**) and orthopyroxene (**d**). Literature $D^{pl/melt}$ values in dacitic and rhyolitic melts (Arth 1976; Nath and Crecraft 1985; Severs et al. 2009), $D^{amph/melt}$ values in andesitic and dacitic melts (Brenan et al. 1995; Sisson 1994; Klein et al. 1997; Hilyard et al. 2000), $D^{gt/melt}$ values in andesitic and dacitic melts (Arth 1976; Klein et al. 2000; Koepke et al. 2003; Klemme et al. 2002; Rubatto and Hermann 2007) and $D^{opx/melt}$ values in andesitic and dacitic melts (Arth 1976; Philpotts and Schnetzler 1970; Schnetzler and Philpotts 1970) are shown for comparison

represent melt composition likely produced by low degree of melting. For mineral/melt partitioning, we used $D^{amphibole/melt}$, $D^{orthopyroxene/melt}$, and $D^{garnet/melt}$ values of this study, $D^{plagioclase/melt}$ of Severs et al. (2009) and $D^{rutile/melt}$ of Xiong et al. (2005). $D_{REE}^{plagiolcase/melt}$ values not given by Severs et al. (2009) were estimated by the lattice strain model (Blundy and Wood 1994). $D^{cpx/melt}$ and $D_{Nb}^{ilm/melt}$ values were estimated by $D_{REE,Y}^{amph/cpx} = 3.0$, $D_{Zr,Hf}^{amph/cpx} = 1.0$ and $D_{Nb}^{ilm/amph} = 30$ (Nehring et al. 2010). Bulk partition coefficients for a residue of amphibolite (Pl + Amp ± Gt ± Ilm ± Rut), two-pyroxene granulite (Pl + Cpx + Opx ± Amp ± Ilm ± Rut) and garnet granulite (Pl + Cpx + Gt ± Amp ± Rut) estimated by Eq. 3 are presented in Electronic Appendix 5b-d. A comparison of bulk D values obtained by Eqs. 2 and 3 (Electronic Appendix 6) indicates that the two approaches provide similar results for most of the elements.

Discussion

Approach to equilibrium

The duration of 1 week (~168 h) for our experiments at 800–1,050 °C is sufficient for approaching equilibrium, according to former melting experiments (Beard and Lofgren 1991; Sen and Dunn 1994; Springer and Seck 1997; Skjerlie and Patino Douce 2002; Xiong et al. 2005). The mineral and melt compositions at different sites in the capsule are homogeneous, with relative standard deviations <15 % for both major and trace elements (Tables 3, 4, 5), and show regular variations with temperature, pressure, and melt proportion (Figs. 4, 5, 6, 7, 8). Melt proportions estimated by mass balance and by assuming $D_{Cs}^{bulk} = 0$ are in good agreement (Electronic Appendix 1a), and the mineralogy of the experiments did not produce any unexpected, metastable phase. The presence of minor zoning in

pyroxene demonstrates that complete equilibrium was not reached. Nevertheless, mineral/melt partition coefficients obtained in our experiments agree well with other experiments. Close to equilibrium is further indicated by similarities between the experimental and literature Fe–Mg exchange coefficient $\left[K_D^{\mathrm{Fe-Mg}} = (\mathrm{FeO/MgO})_{\mathrm{mineral}}/(\mathrm{FeO/MgO})_{\mathrm{melt}}\right]$ for Fe–Mg minerals. The clinopyroxene-melt $K_D^{\mathrm{Fe-Mg}}$ values (0.32 ± 0.05) are close to that determined by Grove et al. (1997) (0.20–0.37, ave. 0.25 ± 0.09) at similar temperatures in andesitic–rhyolitic melts and that determined by Kinzler (1997) and Gaetani and Grove (1998) (0.33–0.36) at 1,100–1,500 °C in basaltic melts. The amphibole-melt $K_D^{\mathrm{Fe-Mg}}$ values (0.43 ± 0.06) are similar to that measured by Alonso-Perez et al. (2009), Grove et al. (1997), and Sen and Dunn (1994) (0.38 ± 0.04, 0.35 and 0.55–0.62, respectively) in andesitic–rhyolitic melts and by Sisson and Grove (1993) (0.35–0.38) in basaltic melts. The orthopyroxene-melt $K_D^{\mathrm{Fe-Mg}}$ (0.41 ± 0.08) is slightly higher than that determined by Grove et al. (1997) and Sisson et al. (2005) (0.29 ± 0.16 and 0.36 ± 0.02, respectively) in andesitic–rhyolitic melts and that by Kinzler (1997) and Gaetani and Grove (1998) (0.32–0.33) in basaltic melts. The garnet-melt $K_D^{\mathrm{Fe-Mg}}$ (0.68–1.22) is in agreement with Sen and Dunn (1994) (0.8–0.6) and Alonso-Perez et al. (2009) (0.78–0.92) in andesitic–rhyolitic melts. Also, the garnet-melt $K_D^{\mathrm{Fe-Mg}}$ decreases with increasing temperature and reaches 1.0 ± 0.2 at 800–900 °C, in agreement with Rubatto and Hermann (2007), who demonstrated that garnet is more Fe-rich than melt at 800–900 °C but becomes more Mg-rich at 1,000 °C. In addition, the plagioclase-melt Na–Ca exchange coefficient $\left[K_D^{\mathrm{Na-Ca}} = (\mathrm{Na_2O/CaO})_{\mathrm{plagioclase}}/(\mathrm{Na_2O/CaO})_{\mathrm{melt}}\right]$ (0.42–0.67) is similar to that of Beard and Lofgren (1991) (0.45–0.52) in dacitic-rhyolitic melts.

Temperatures estimated by the Ti-in-melt thermometer (Hayden and Watson 2007) are within ±50 °C (except for the 1,050 °C experiment). For the high temperature (1,000–1,050 °C) experiments, differences between the experimental temperatures and that estimated by the two-pyroxene thermometer (Wood and Banno 1973; Brey and Köhler 1990) are within ±40 °C, indicating that equilibrium is approached. For the lower temperature experiments (800–900 °C), two-pyroxene thermometry reproduces experimental temperatures within ±90 °C.

Comparison of phase relations with previous experiments

This study mainly concerns the appropriate *P–T* conditions of forming adakite/TTG magmas by anatexis of mafic lower continental crust. A variety of residues such as (garnet) amphibolite, two-pyroxene granulite, garnet granulite, and garnet pyroxenite were produced in our partial melting experiments (Fig. 2; Table 2). This provides a good opportunity to evaluate how melt compositions (especially incompatible elements) are influenced by residual assemblages. The obtained results can be compared with a wealth of experiments that exist in mafic rock–water systems. It is important to note that while in detail the results will differ due to different SiO_2, alkali and water contents and Mg# of the starting materials, the broad trends are comparable.

The solidus temperature at 10 kbar is between 750 and 800 °C (Fig. 2), close to that of Rushmer (1991) (~800 °C) at 8 kbar and that of Wyllie and Wolf (1993) and Lopez and Castro (2001) at 10 kbar in dehydration-melting of amphibolites. It is 100–150 °C higher than the wet solidus of basaltic system (Lambert and Wyllie 1972; Green 1982) and the actual solidus (650–750 °C) determined by Wolf and Wyllie (1994) for a calcic amphibolite. The experimental garnet-in curve at 900 °C is between 10 and 12.5 kbar (Fig. 2), similar to that of the former dehydration-melting experiments (Green 1982; Winther and Newton 1991; Wyllie and Wolf 1993; Wolf and Wyllie 1994; Springer and Seck 1997; Nakajima and Arima 1998; Lopez and Castro 2001; Skjerlie and Patino Douce 2002). The positive dP/dT slope of the garnet-in curve at 900–1,000 °C is consistent with former results (Green 1982; Sen and Dunn 1994; Springer and Seck 1997; Nakajima and Arima 1998). The absence of garnet at 10–12.5 kbar and 800 °C was probably due to reluctance of garnet nucleation in unseeded experiments below 900 °C (Wyllie and Wolf 1993; Wolf and Wyllie 1994). The amphibole-out curve is located between 950 and 1,000 °C (Fig. 2). In former dehydration-melting of basaltic compositions at 8–15 kbar, the amphibole-out curve was constrained to lie between 950 and 1,000 °C (Rushmer 1991; Wyllie and Wolf 1993; Wolf and Wyllie 1994; Liu et al. 1996) or between 1,000 and 1,100 °C (Green 1982; Sen and Dunn 1994; Rapp 1995; Rapp and Watson 1995; Springer and Seck 1997). The plagioclase-out curve is above 12.5 kbar between 900 and 1,000 °C, with a negative dP/dT slope in agreement with previous work (Green 1982; Sen and Dunn 1994; Liu et al. 1996). The clinopyroxene-in curve, upright at ~850 °C, has a slightly negative dP/dT slope based on extrapolation of clinopyroxene abundances at 900 °C. The orthopyroxene-in curve has a positive dP/dT slope and is between 800 and 900 °C at 10–12.5 kbar and between 1,000 and 1,050 °C at 15 kbar. The ilmenite-rutile transition has a negative dP/dT slope. The minimum pressure of rutile stability (10 kbar at 1,000 °C) is 2.5–5 kbar lower than that determined in some experiments (Liu et al. 1996; Xiong et al. 2005, 2009; Xiong 2006), but is in good agreement with the results of Patino Douce and Beard (1995).

Comparison of major elements between partial melts and natural adakite/TTG

The experimental partial melts change from granodiorite to tonalite with the increase in melting degree (Fig. 5), similar to that observed by Helz (1976) and Sen and Dunn (1994), but is different from some other experiments which produced melts varying from trondhjemite to tonalite (Rapp et al. 1991; Winther and Newton 1991; Winther 1996; Springer and Seck 1997). In the major oxides versus MgO diagrams (Fig. 6), the partial melts mostly (except that produced at 15 kbar and 1,050 °C) resemble pristine adakite/TTG in MgO, SiO_2, Al_2O_3, FeO^T, K_2O, and A/CNK. The melts tend to have slightly elevated CaO and slightly lower Na_2O with respect to the natural rocks. Mass balance calculations indicated that there was up to 30 % Na_2O loss in the hydrous glasses in some runs, which would shift some melts to higher Na_2O contents. However, the main reason that the melts do not plot into the trondhjemite field is related to the CaO contents of the melts (Fig. 5). The CaO contents in melt increase with increasing temperature (Fig. 7) in agreement with experimental results presented by Rapp and Watson (1995). Hence, trondhjemite melts are preferentially formed at low temperatures involving small melt fractions. At similar MgO contents, TiO_2 of the 800–900 °C melts (0.2–1.0 wt%) is similar to that of natural adakite/TTG rocks, whereas TiO_2 of the 1,000–1,050 °C partial melts (1.2–1.6 wt%) is conspicuously higher. This is in agreement with Xiong et al. (2009), who suggest that 750–950 °C is the most likely temperatures for producing the Ti content of TTG and higher temperatures produce melts too rich in TiO_2. Variations of TiO_2 with MgO (Fig. 6b) and temperature (Fig. 7c) also agree with former experiments (Ryerson and Watson 1987; Hayden and Watson 2007; Xiong et al. 2009). Based on the TiO_2 and MgO of the partial melts, it is suggested that pristine adakite/TTG magmas were most likely produced by low to moderate degrees (<40 %) of partial melting of hydrous basalts. Similarly, it is observed that TTG rocks from some Archean terranes were formed by 10–30 wt% melting of amphibolite at 750–900 °C (Nehring et al. 2009, 2010).

According to Xiong et al. (2009), about 0.8–1.0 wt% TiO_2 in the protolith is required for rutile saturation at low degrees (<20 wt%) of melting. Some other experiments (Sen and Dunn 1994; Rapp and Watson 1995; Rapp et al. 1999; Alonso-Perez et al. 2009) also show that Ti-rich phases are stable during 10–40 % melting of a mafic protolith with 0.9–1.2 wt% TiO_2. Ilmenite and titanite are present in some natural granulites which may represent residue of 10–30 % melting of amphibolites with 0.7–1.5 wt% TiO_2 (Storkey et al. 2005; Nehring et al. 2009). Consequently, it is expected that Ti-rich phases should be present at low to moderate degrees of melting of mafic lower crust, which usually has 0.8–1.3 wt% TiO_2 (Rudnick and Gao 2003 and references therein).

A major difference between intra-continental adakites and the circum-Pacific arc adakites is that the former usually possess higher K_2O/Na_2O ratios (>0.5). This has been ascribed to elevated K_2O/Na_2O in the protolith (Zhang et al. 2001; Rapp et al. 2002; Xiao and Clemens 2007), assimilation and fractional crystallization (AFC; Rapp et al. 2002) or high-pressure melting (Xiao and Clemens 2007). K_2O/Na_2O of our melts decreases from 0.8 to 0.5–0.3 when melting degree increases from 14.5 to 30–40 %, indicating that K is highly incompatible during partial melting. Thus, low-degree melting may be an additional important factor responsible for the high K_2O/Na_2O of many intra-continental adakites. K_2O/Na_2O of the source will determine whether granodioritic or trondhjemitic melts are formed. Since the mafic lower crust (Condie and Selverstone 1999; Rudnick and Gao 2003 and references therein) contains significant amounts of K_2O, small to moderate degrees of melting should produce granodiorite and tonalite but not trondhjemite. This indicates that the protoliths of natural trondhjemites and most circum-Pacific arc adakites are more sodic than our starting material and could be produced either from lower crustal protoliths (e.g., Condie 2005; Rollinson 2012) deficient in K_2O or by partial melting of K-poor mafic rocks in subducted slabs.

If converted to amphibolite, our starting material contains about 60 wt% amphibole, 30 wt% plagioclase, 10 wt% quartz, and accessory ilmenite and apatite. This fictive amphibolite should contain about 1.2 wt% H_2O under fluid-absent conditions (assuming 2.0 wt% structural H_2O in amphibole), similar to that of natural amphibolites (1–2 wt% H_2O) (Rapp et al. 1991; Rushmer 1991; Sen and Dunn 1994; Rapp and Watson 1995). Our 1,000–1,050 °C experiments have 1.5–2.0 wt% H_2O and thus can be used to monitor fluid-absent melting under natural conditions. Our 800–900 °C experiments with 4–6 wt% H_2O should represent melting by addition of an aqueous fluid phase. The fact that our 800–900 °C melts closely match the natural adakite/TTG in a wide range of major elements suggests that adakite/TTG melts might have been generated under hydrous conditions.

Phase control on the trace element signature of adakite/TTG

Adakite/TTG rocks are characterized by high Ba and Sr (usually >400 ppm), low Y (<18 ppm) and HREE (Yb <1.9 ppm), elevated La/Yb (>10) and Sr/Y (mostly >40), strongly depleted Nb, Ta, and Ti, and lack of negative Sr and Eu anomalies (Martin 1986, 1999; Defant and Drummond 1990; Condie 2005; Martin et al. 2005). These geochemical features have been attributed to the presence

of garnet and Ti-rich phases and lack of plagioclase in the residue. Ti-rich phases such as rutile, ilmenite, and titanite contain high amounts of Ti, Nb, and Ta (Green and Pearson 1987; Stimac and Hickmott 1994; Storkey et al. 2005; Xiong et al. 2005; Nehring et al. 2010; John et al. 2011). Varying modal ratios of titanite over rutile (John et al. 2011) or abundant low-magnesium amphibole (Foley et al. 2002) in the residue have been taken to account for the Nb/Ta and Zr/Sm characteristics of adakite/TTG rocks. It is interesting to note that amphibole preferentially incorporates Nb over Ta with respect to melt in the 12.5 kbar, 900 °C experiment (Fig. 10b). Thus, residual amphibole is likely responsible for preferential enrichment of Ta in some of the melts, in agreement with the study of Tiepolo et al. (2007). Titanite and allanite also carry high amounts of REE, Th, and U and play an important role in controlling the distribution of these elements during partial melting of amphibolite (Hermann 2002; Storkey et al. 2005). Allanite is not stable at high temperatures as LREE enter into the melt (Hermann 2002). In our experiments, ilmenite and rutile are present at 10–40 % melting, while allanite and titanite are present only at 15 kbar and 800 °C. Apatite is present only in a few of our experiments but should be close to saturation in the 800–1,000 °C melts, based on apatite solubility calculations using the equation of Harrison and Watson (1984). Zircon is far from saturation in the 900–1,050 °C melts, but is close to saturation in the 800 °C melts according to the zircon solubility equation of Watson and Harrison (1983). Considering that P and Zr contents in our starting material are close to that of mafic lower crust (Table 1), small amounts of apatite and zircon are potentially stable during initial partial melting of lower crust.

Trace element modeling

Our starting material closely matches average lower crust in major elements and trace elements such as Y, Sr, and Zr. However, the REE, Cs, Nb, Ta, Hf, Th, and U contents of the starting material have been increased to obtain better measurement of these important elements in relatively small melt pools. Therefore, the obtained trace element patterns of the melt cannot be directly compared with trace element patterns of adakites and TTG. Bulk partition coefficients determined by Eqs. 2 and 3 (Electronic Appendix 5) were used to model the trace element contents of partial melts from average compositions of mafic lower crust (Table 1). We used the batch melting equation

$$C_i^{\text{melt}} = C_i^{\text{LC}} / \left[D_i^{\text{bulk}} + F(1 - D_i^{\text{bulk}}) \right] \quad (4)$$

in which C_i^{LC} and C_i^{melt} represent the concentrations of element i in lower crust and partial melt, respectively, and F is the weight fraction of partial melt. The modeling was made in several schemes and the results are shown in the primitive mantle-normalized spidergrams (Fig. 11, Electronic Appendix 7). First, the actual melt fractions (Table 2), D_i^{bulk} values calculated by Eq. 2 (Electronic Appendix 5a) and lower crust of RG2003 were used. This provides the most direct way to compare our experimental results with adakite/TTG rocks (Fig. 11a, Electronic Appendix 8). In a second step, CS1999 was used as protolith to examine the effect of source variation on the partial melts (Fig. 11b). These two data sets do not permit to deconvolute the influence of different melt fractions on the melt composition. To constrain this problem, partial melts produced by 5, 10, 20 to 40 wt% melting at 12.5 kbar and 900 °C were modeled using RG2003 and D_i^{bulk} values derived from Eq. 3 (Electronic Appendix 5c), to examine the influence of melt fraction variations on the trace elements of melts (Fig. 11c). In a next step, the influence of phase assemblage in the residue was evaluated. We modeled the trace elements of 10 wt% melts which are in equilibrium with amphibolite, two-pyroxene granulite, and garnet granulite (Fig. 11d), using lower crust of RG2003 and bulk partition coefficients given in Electronic Appendix 5d. Melts from 20 wt% melting of RG2003 at the experimental P–T conditions were further modeled, using D_i^{bulk} values estimated by Eqs. 2 and 3, respectively (Electronic Appendix 7). This set of models allows a thorough evaluation on the influence of melt fraction, source composition, and residual mineral assemblage on trace elements of the partial melt.

Partial melts obtained from RG2003 at 10–12.5 kbar and 800–900 °C and 15 kbar and 800 °C closely resemble natural adakite/TTG in trace elements (Fig. 11a–d; Electronic Appendix 7). Partial melts obtained at 10–12.5 kbar and 1,000 °C and 15 kbar and 1,050 °C have elevated HREE. In contrast, partial melts obtained at 13.5–15 kbar and 900 °C and 15 kbar and 1,000 °C have strongly depressed HREE, below that of natural adakite/TTG. In addition, melts obtained at 10 kbar and 1,000 °C have obvious Sr and Eu depletions. An additional comparison between the modeled melts and natural adakite/TTG is illustrated in the chondrite-normalized La/Yb-Yb, La/Yb-La, Gd/Yb-Yb, and Sr/Y-Y plots (Fig. 12).

As indicated by Eq. 4, melt fraction and residual minerals provide important controls on trace elements of the partial melts. Highly incompatible elements such as Rb, Ba, Th, U, La, and Ce have approximately inverse correlations with melt fraction. For example, La abundances in melts derived by 10–40 wt% melting of RG2003 at 12.5 kbar and 900 °C are within the range of natural adakite/TTG (10–60 ppm), but are significantly higher at 5 wt% melting (Fig. 12b). As melt fraction increasing from 5 to 40 wt%, Rb, Ba, Th, U, La, and Ce in the modeled

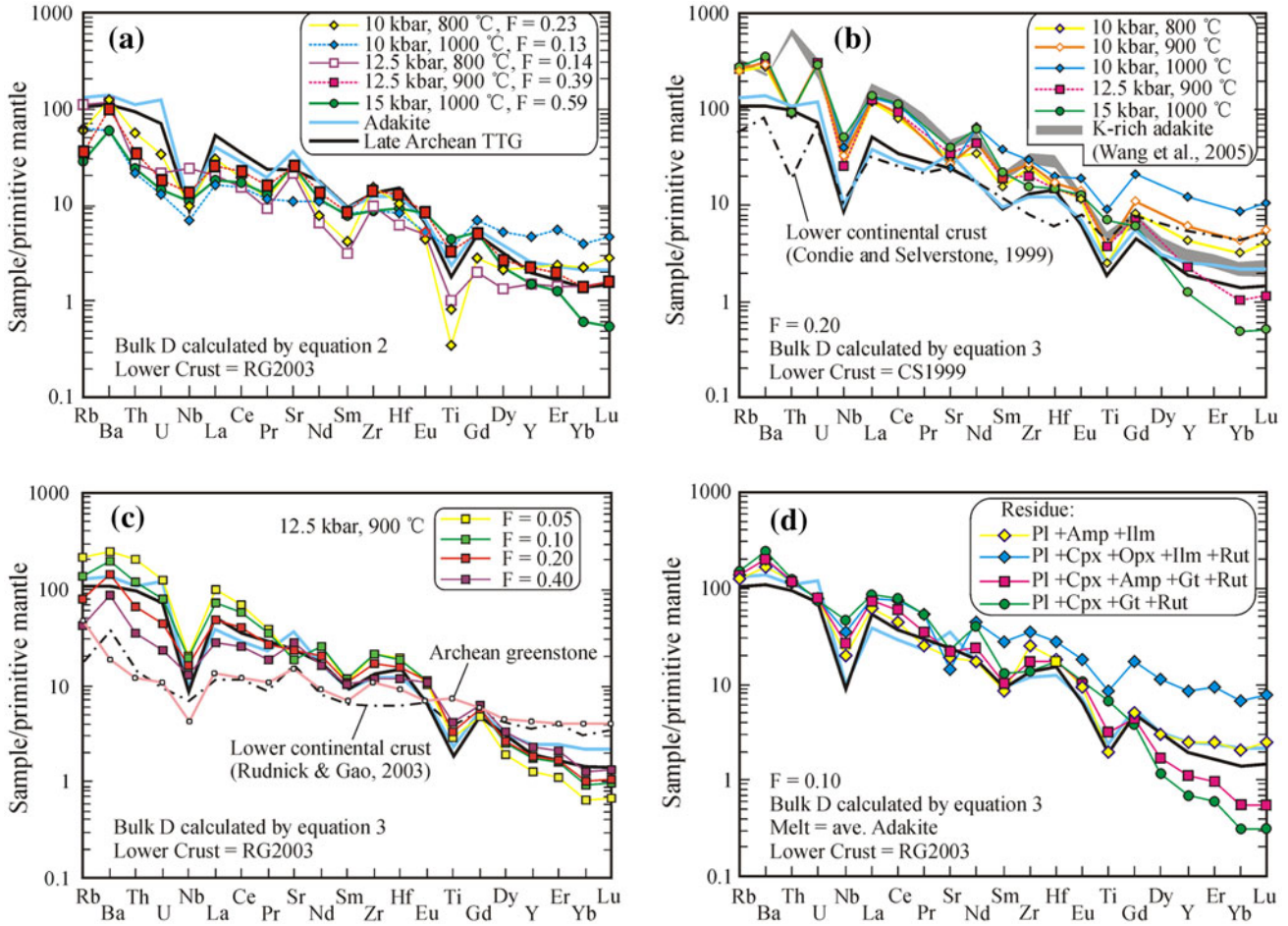

Fig. 11 Primitive mantle-normalized spidergrams for modeled melts from mafic lower crust (RG2003, Rudnick and Gao 2003; CS1999, Condie and Selverstone 1999). **a** Melts produced from RG2003 at *P–T* conditions of 10 kbar and 800 °C, 10 kbar and 1,000 °C, 12.5 kbar and 800 °C, 12.5 kbar and 900 °C and 15 kbar and 1,000 °C. The actual melt fractions (F) of the experiments (Table 2) were used for the modeling. **b** Melts produced from CS1999 at *P–T* conditions of 10 kbar and 800 °C, 10 kbar and 900 °C, 10 kbar and 1,000 °C, 12.5 kbar and 900 °C and 15 kbar and 1,000 °C, with $F = 0.20$. Note that the modeled melts are similar to the K-rich adakites from Hohxil in northern Tibet (Wang et al. 2005) in highly incompatible elements except for Th. **c** Melts produced from RG2003 at 12.5 kbar and 900 °C, with *F* varying from 5, 10, 20 to 40 wt%. **d** Melts produced by 10 % melting of RG2003, with residual assemblages of Pl + Amp + Ilm, Pl + Cpx + Opx + Ilm + Rut, Pl + Cpx + Amp + Gt + Rut, and Pl + Cpx + Gt + Rut. For the modeling, D_i^{bulk} values obtained by Eq. 2 were used in **a**, whereas D_i^{bulk} values calculated by Eq. 3 were used in **b**, **c** and **d**. Average late Archean TTG (Condie 2005), average adakites (Electronic Appendix 8), late Archean basalt from the Superior greenstone belt (sample SC95-24, Polat and Kerrich 2001) and lower crust compositions of Rudnick and Gao (2003) and Condie and Selverstone (1999) are shown for comparison. Data of primitive mantle are after Sun and McDonough (1989)

melts at 12.5 kbar and 900 °C decrease by a factor of 3–6, accompanied by a slight increase in HREE (Figs. 11c, 12). In contrast, elements with large D^{bulk} values are mainly controlled by residue assemblages. HREE of melts derived from RG2003 are depressed below that of most natural adakite/TTG when garnet in the residue is >20 % ($D_{Yb}^{bulk} > 6.0$, given $D_{Yb}^{Garnet/melt} = 30$). The Gd to Lu distribution is relatively flat when residual amphibole is high in proportion. Melts from RG2003 have a positive Sr anomaly when residual plagioclase is <20 % but a negative Sr anomaly when residual plagioclase is >30 %.

Source composition exerts a primary control on geochemical features of the partial melt (Clemens and Stevens 2012). At given D_i^{bulk} and melting degree, partial melts from CS1999 should have incompatible elements about 1.1–3.4 times higher than that from RG2003. Modeled melts produced by 10–40 % melting of lower crust at 10–12.5 kbar and 900 °C have Sr about 330–800 ppm, similar to that of natural adakite/TTG. Modeled melts produced from lower crust at 10–15 kbar resemble natural adakite/TTG in Sr/Y ratio (Fig. 12d). A special type of K-rich adakites, which have elevated LREE and lower Th compared to most natural adakite/TTG, has been reported from the Hohxil area in northern Tibet (Wang et al. 2005). In most of the trace elements (except Th), the Hohxil adakites resemble modeled melts derived by 20–40 wt%

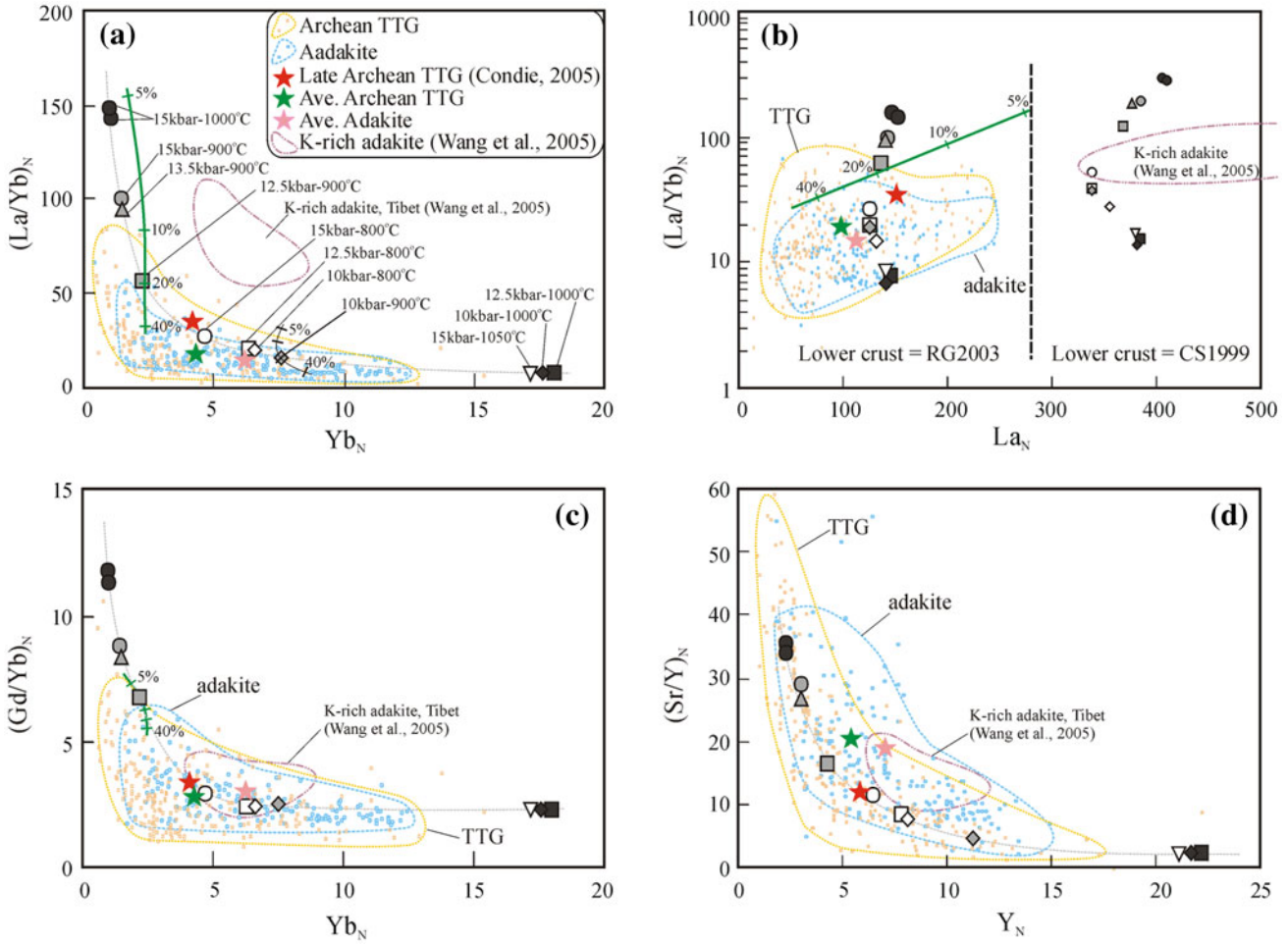

Fig. 12 $(La/Yb)_N$ versus Yb_N (**a**), $(La/Yb)_N$ versus La_N (**b**), $(Gd/Yb)_N$ versus Yb_N (**c**) and $(Sr/Y)_N$ versus Y_N (**d**) diagrams for modeled melts produced by 20 wt% melting of lower crust (Rudnick and Gao 2003). Melts from lower crust of Condie and Selverstone (1999) is also shown in **b**. D_i^{bulk} values calculated by Eq. 3 were used for the modeling. Symbols for partial melts are the same as in Fig. 5. Late Archean TTG (Condie 2005) and averages of 316 Archean TTG and 204 lower crust-derived adakites (see Fig. 6 for data sources) are illustrated for comparison. Melts from 5 to 40 wt% melting of RG2003 at 12.5 kbar and 900 °C and 10 kbar and 900 °C are also shown (*green lines with tag marks*). Note that at 12.5 kbar and 900 °C La and La/Yb decrease significantly with the increase of melting while Yb and Gd/Yb variations are small. Melts produced by 20 wt% melting of mafic lower crust at 13.5 kbar and 900 °C and 15 kbar and 900–1,000 °C have lower Yb and higher La/Yb and Gd/Yb than most natural adakite/TTG rocks. The K-rich adakites from Hohxil in northern Tibet (Wang et al. 2005) have considerably high La and La/Yb but similar Gd/Yb and Sr/Y values compared to most of the other adakite/TTG rocks. N means chondrite normalization (Sun and McDonough 1989)

melting of CS1999 at 10–12.5 kbar and 800–900 °C and 15 kbar and 800 °C (Figs. 11b, 12b), indicating that the Hohxil adakites were probably derived from a source compositionally similar to CS1999, but higher in Th.

It is important to note that mafic lower crust is characterized by enriched Ba and Sr, depleted Nb, Ta, and Ti, depressed HREE, and fractionated REE (Fig. 11b, c). These geochemical features may be more or less inherited by the partial melts. Therefore, for producing adakite/TTG from lower crust, it does not necessarily require the stability of rutile, high amounts of garnet, and absence of plagioclase in the residue. Arc-like basaltic rocks, although volumetrically subordinate, are widespread in the Archean greenstone belts (Hollings and Kerrich 2000; Polat and Kerrich 2001; Polat et al. 2005; Smithies et al. 2009). These rocks resemble mafic lower crust in trace elements (Fig. 11c) and thus may serve as the sources of Archean TTG (Smithies et al. 2009; Adam et al. 2012; Nagel et al. 2012).

Based on above discussions, the high Ba, Sr, La, La/Yb, and Sr/Y and low Y and Yb features of adakite/TTG do not necessarily signify high-pressure melting. These features could result from magma source composition, small degree of melting or fractionation/accumulation of plagioclase. Instead, Gd/Yb may be taken as a more credible index of melting pressure, as Gd/Yb is much more sensitive to the proportion of residual garnet than to the other factors. According to Nair and chacko (2008), at least 20 wt%

garnet is required in the residue in order to generate the Yb depletion of TTG by 20 % melting of MORB. In contrast, our modeling indicates that magmas produced by 20–40 wt% melting of lower crust at 13.5 kbar and 900 °C and 15 kbar and 900–1,000 °C (25–50 wt% garnet in the residue) have lower Yb (≤0.3 ppm) and higher Gd/Yb (≥8.0) compared to natural adakite/TTG rocks, which mostly have Yb >0.3 ppm and Gd/Yb <6.0 (TTG and adakites have Gd/Yb ratios of 3.6 ± 1.8 and 3.4 ± 1.1, respectively; Fig. 12c).

Pressure, temperature, and H_2O conditions of producing adakite/ TTG from lower crust

To account for the depletions of Nb, Ta, and HREE and lack of negative Sr and Eu anomalies of adakite/TTG, previous work has suggested that the residue must contain rutile and high amounts (>20 wt%) of garnet and insignificant plagioclase (Defant and Drummond 1990; Peacock et al. 1994; Martin 1999; Martin et al. 2005; Xiong et al. 2005, 2009; Nair and Chacko 2008). A series of partial melting experiments consistently demonstrate that pressures of >15 kbar are required for producing adakite/TTG magmas from hydrous MORB, shoshonite, or Archean greenstones (Rapp et al. 1991, 1999, 2003; Sen and Dunn 1994; Rapp 1995; Rapp and Watson 1995; Xiong et al. 2005, 2009; Clemens et al. 2006; Xiong 2006; Nair and Chacko 2008; Adam et al. 2012; Laurie and Stevens 2012). Geochemical modeling also indicates a minimum pressure of 15 kbar for forming the high Sr/Y signature of adakite from MORB sources (Moyen 2009). A higher minimum pressure of ~20 kbar is suggested by near-liquids experiments and partial melting experiments using high-K basalts (Xiao and Clemens 2007; Coldwell et al. 2011). In these studies, the partial melting residues are mainly eclogite.

An alternative model proposes that adakitic melts could be formed from basaltic arc magma by fractionation of a garnet-bearing assemblage (Macpherson et al. 2006). The garnet fractionation may happen either in the deep crust via formation of garnet gabbros or in the upper mantle via formation of garnet pyroxenites (Alonso-Perez et al. 2009). The high-pressure fractionation typically leads to a progressive depletion of HREE with increasing SiO_2 of the melts, and broom-like chondrite-normalized REE distributions (Macpherson et al. 2006). However, such kind of geochemical features are lacking in most adakite/TTG rocks. Mass balance indicates that, in order to form adakite/TTG rocks with 70 wt% SiO_2 from a basaltic magma with 50 wt% SiO_2, it requires a fractionation of more than 60 % garnet + amphibole (the degree should be higher if accompanied by pyroxene fractionation). Such high degrees of fractionation may not be favored by the viscosity of magma and also cannot explain the somewhat unique geochemistry of adakite/TTG and the lack of transitional rocks. Therefore, although fractional crystallization is reported to be a major mechanism in a few cases, it is unlikely volumetrically important in forming adakite/TTG.

This paper concentrates on the most favorable *P–T* range of producing adakite/TTG by partial melting of lower crust. Our experiments demonstrated that partial melts similar to adakite/TTG in major and trace elements can be formed by 10–40 wt% melting of mafic lower crust (Rudnick and Gao 2003) at 10–12.5 kbar and 800–900 °C and 15 kbar and 800 °C. The residues are (garnet) amphibolite, two-pyroxene granulite, or garnet granulite. The results are in agreement with Springer and Seck (1997), who suggested that partial melts similar to adakite/TTG in REE can be produced from lower crust at 10–12.5 kbar but not at higher pressures. A similar pressure range of 10–14 kbar has also been proposed by the geochemical modeling of Nagel et al. (2012) for producing TTG from arc tholeiites. On the other hand, our modeled melts from 10 to 40 % melting of lower crust at 13.5 kbar and 900 °C and 15 kbar and 900–1,000 °C have depressed Yb (<0.3 ppm) and elevated La/Yb and Gd/Yb compared to natural adakite/TTG rocks (Fig. 12), due to high amounts of garnet (>20 %) in the residue. This means that a depth of >45–50 km is not favorable for producing adakite/TTG from mafic lower crust. The Miocene K-rich adakites from Hohxil in northern Tibet (Wang et al. 2005) are similar to most natural adakite/TTG in Yb, Y, Gd/Yb, and Sr/Y values despite the elevated La and La/Yb (Fig. 12), indicating that they were formed at a similar but not higher depth.

Adakite/TTG rocks typically form a concave parabolic trend in the La/Yb-Yb and Sr/Y-Y plots (Martin 1986, 1999; Defant and Drummond 1990; Condie 2005; Moyen 2011). The samples with low Y and high Sr/Y have been widely interpreted to signify high-pressure melting. However, we recognized that adakite/TTG samples with highly different Y, Yb and Sr/Y values usually have similar Gd/Yb (mostly <5), indicating a similar pressure of melting.

A high temperature range of 1,000–1,100 °C has been proposed for producing adakite/TTG melts (Rapp and Watson 1995; Rapp et al. 1999; Xiao and Clemens 2007). Xiong et al. (2009) suggested that 750–950 °C is the most likely temperatures for producing TTG because higher temperatures produce melts too rich in TiO_2. Our results also show that the 800–900 °C melts have TiO_2 (0.2–1.0 wt%) similar to that of natural adakite/TTG rocks, whereas the 1,000–1,050 °C partial melts have conspicuously higher TiO_2 (1.2–1.6 wt%).

Based on these data, we suggest that the most appropriate *P–T* conditions for producing adakite/TTG from lower crust (Rudnick and Gao 2003) should be

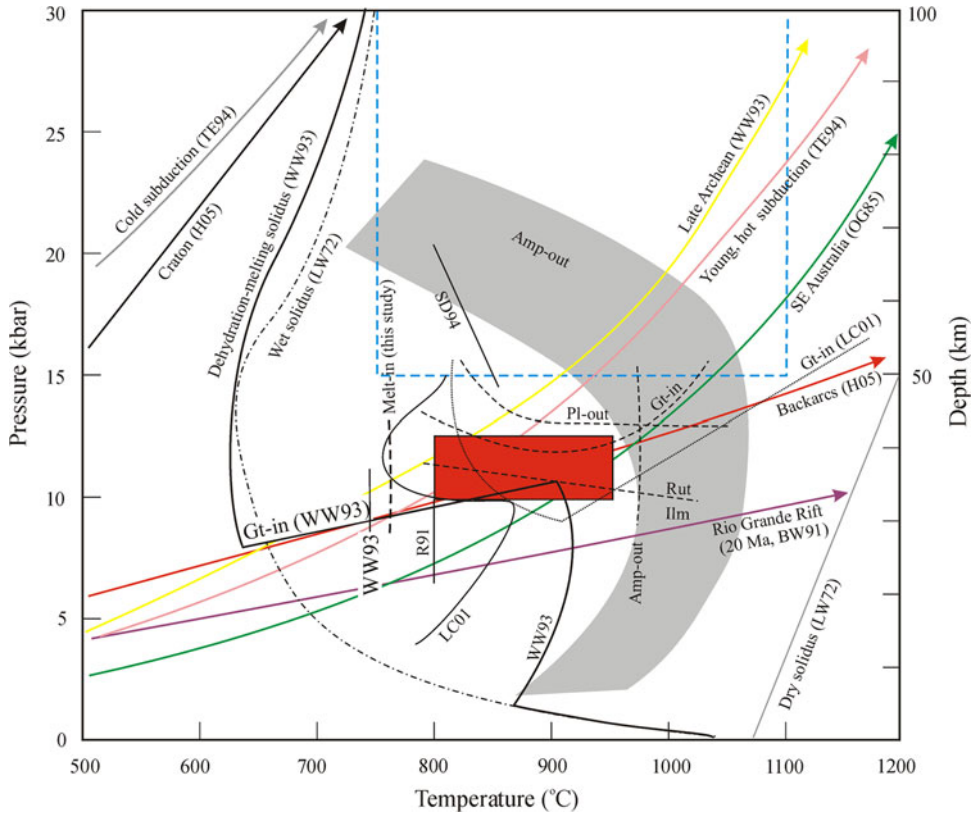

Fig. 13 Pressure–temperature conditions (*red box*; 10–12.5 bkar and 800–950 °C) appropriate for formation of adakite/TTG from mafic lower crust. The *blue dashed line* encloses the *P–T* conditions formerly proposed for adakite/TTG formation by partial melting of subducted oceanic crust (see text for the references). The *gray area* incorporates the amphibole-out boundaries determined in former experiments (see Xiong et al. 2009 and references therein). *Arrows* geotherms; *Dashed lines* phase boundaries obtained in this study; *Black solid lines* dehydration-melting solidi. Data sources: BW91, Bussod and Williams (1991); H05, Hyndman et al. (2005); LC01, Lopez and Castro (2001); LW72, Lambert and Wyllie (1972); OG85, O'Reilly and Griffin (1985); R91, Rushmer (1991); SD94, Sen and Dunn (1994); TE94, Thompson and Ellis (1994); WW93, Wyllie and Wolf (1993)

10–12.5 kbar and 800–950 °C (Fig. 13). A similar *P–T* range was proposed by Peacock et al. (1994) for producing adakites by water-undersaturated melting at the base of arcs. This *P–T* range is close to the peak metamorphic conditions of some mafic granulite xenoliths (Hacker et al. 2000; Liu et al. 2001, 2003) and granulite terranes (Storkey et al. 2005; Nehring et al. 2009, 2010), part of which may represent residue of adakite/TTG magmas (Jiang et al. 2007; Storkey et al. 2005; Nehring et al. 2009, 2010). Such conditions can be reached at 30–40 km depth with a geothermal gradient of 20–30 °C/km, close to that of late Archean, hot subduction regions, and continental extension regions such as subduction zone backarcs (Bussod and Williams 1991; Wyllie and Wolf 1993; Thompson and Ellis 1994; Hyndman et al. 2005; Fig. 13). To our knowledge, adakites with geological, geochronological, and isotopic evidences indicating a lower crust origin usually occur in extensional settings and are accompanied with contemporaneous mafic magmatism (Petford and Atherton 1996; Chung et al. 2003; Hou et al. 2004; Wang et al. 2005, 2006; Xu et al. 2006; Guo et al. 2007; Karsli et al. 2010; Qian and Hermann 2010; Zhang et al. 2010). The mafic magmas may have a density close to that of lower crust and thus be forced to undergo fractional crystallization at 8–15 kbar (Green 1982; Bussod and Williams 1991), providing heat for lower crustal melting.

The role of water in the melting process remains to some extent enigmatic. Melt fractions are very low at 800–900 °C (likely <5 %) because reactions consuming amphibole are limited. Our modeling suggests that LILE and LREE of such melts are too high with respect to adakites and TTG. The melt fraction during amphibole breakdown such as encountered between 900 and 1,000 °C produces 10–40 % melt. However, TiO_2 contents of the 1,000 °C melts which have H_2O in the starting material close to that of natural amphibolites are significantly higher than what is observed in natural adakite/TTG rocks. The best match between modeled melts and adakite/TTG derived from lower crustal anatexis is obtained when partial melting is related to addition of minor amounts of aqueous fluids. For a hot subduction setting and a back-arc setting, the addition of an aqueous fluid phase is feasible. It

is more difficult to explain such a process during intracontinental rifting. It has to be evaluated by future studies whether such aqueous fluids can be liberated from crystallizing hydrous mafic melts or from hydrous ultramafic rocks. Alternatively, dehydration of ultramafic, chlorite-rich lithologies could provide a source for aqueous fluids at lower crustal conditions (Fumagalli and Poli 2005).

Geological implications

Felsic magmas similar to adakite/TTG in major and trace elements can be formed by partial melting of either subducted oceanic slab or mafic lower crust. High-PT experiments and geochemical analysis consistently demonstrate that adakite/TTG from MORB, shoshonite, and Archean greenstones were formed at pressures of >15 kbar (Rapp et al. 1991, 1999, 2003; Sen and Dunn 1994; Rapp 1995; Rapp and Watson 1995; Xiong et al. 2005, 2009; Clemens et al. 2006; Xiong 2006; Nair and Chacko 2008; Moyen 2009; Adam et al. 2012; Laurie and Stevens 2012). A similar depth is widely assumed for producing adakite/TTG rocks from lower crust. This is seemingly well supported by the occurrence of Cenozoic adakites in Andes (Atherton and Petford 1993; Petford and Atherton 1996; Coldwell et al. 2011) and Tibet (Chung et al. 2003; Hou et al. 2004; Wang et al. 2005; Guo et al. 2007) where modern crustal thickness reaches 50–70 km. Accordingly, the occurrence of ancient adakite/TTG which were likely produced by anatexis of lower crust is interpreted to witness an overthickened crust deeper than ~50 km (Zhang et al. 2001; Xu et al. 2002; Clemens et al. 2006; Xiao and Clemens 2007; Huang et al. 2008; Zhao et al. 2008; Smithies et al. 2009; Yu et al. 2012). A delamination model has been proposed for the formation of adakite/TTG from lower crust (e.g., Rapp and Watson 1995; Zegers and van Keken 2001; Kay and Kay 2002; Skjerlie and Patino Douce 2002; Xu et al. 2002; Chung et al. 2003; Gao et al. 2004; Whalen et al. 2004; Bedard 2006; Wang et al. 2006, 2007; Xu et al. 2006, 2008, 2010; Xiao and Clemens 2007; Huang et al. 2008; Karsli et al. 2010; Liu et al. 2010; Zhang et al. 2001, 2007, 2010). In this model, the base of the magmatically or tectonically thickened crust is converted to eclogite and then delaminated into the underlying mantle. Either the delaminated crust or the newly exposed lower crust near the amphibolite/eclogite boundary would be heated to produce the adakite/TTG magmas. Important evidences in favor of the delamination model come from the Mesozoic high-Mg adakites in eastern North China (Gao et al. 2004; Xu et al. 2006, 2008, 2010). These rocks contain dunite and peridotite xenoliths, reversely zoned pyroxenes as well as high MgO, Cr, and Ni. Nevertheless, recent data show that, at least in some cases, such high-Mg diorites were formed by reaction between lower crust-derived magmas and pre-existing dunite and peridotite at crustal depths (Qian and Hermann 2010). Our experiments show that adakite/TTG can be produced from lower crust composition (Rudnick and Gao 2003) at 10–12.5 kbar and 800–950 °C but not at 13.5 kbar and 900 °C and 15 kbar and 900–1,000 °C. Thus, an overthickened crust is not necessarily required for producing adakite/TTG from lower crust. It should be pointed out that our results do not invalidate the former conclusion that a depth of >15 kbar may be required for formation of adakite/TTG from MORB.

Conclusions

We conducted partial melting experiments to constrain the suitable *P–T* conditions for producing the typical major and trace element characteristics of adakite/TTG from mafic lower crust. The results show that adakite/TTG magmas can be formed by 10–40 wt% melting of hydrous mafic lower crust (Rudnick and Gao 2003) at 10–12.5 kbar and 800–900 °C and 15 kbar and 800 °C, leaving a residue of (garnet) amphibolite, two-pyroxene granulite or garnet granulite. Partial melts produced at 13.5 kbar and 900 °C and 15 kbar and 900–1,000 °C from lower crust have depressed Yb and elevated La/Yb and Gd/Yb compared to natural adakite/TTG rocks, due to high garnet amounts in the residue. We suggest that the most likely *P–T* conditions for producing adakite/TTG from an average mafic lower crust composition (Rudnick and Gao 2003) are 30–40 km and 800–950 °C. Although a depth of >50 km may be required for producing adakite/TTG from MORB, a depth of >45–50 km is unfavorable for forming adakite/TTG from lower crust composition, and it is not necessary to transform lower crust into eclogite in order to produce adakite/TTG. There are ample geological, geochronological, and isotopic evidences that partial melting of lower crust is an important process in producing adakite/TTG rocks from the Archean to the present. Our experimental study demonstrates that such rocks cannot be used to witness an ancient overthickened crust. Care has to be taken to use these rocks to advocate lower crustal delamination.

Acknowledgments D. Scott, D. Clark and W.O. Hibberson are acknowledged for technical assistance during the piston-cylinder experiments. We are grateful to F. Brink, C. Allen, G. Hunter, H. Cheng, and L. Li for help during the LA-ICP-MS and SEM analyses. R. Rapp, J.J. Yang, J.H. Guo, F. Liu, H.St.C. O'Neill, and T.G. Lan provided constructive suggestions. J. Adam and two anonymous reviewers provided very helpful comments. We thank J. Hoefs for efficient handling of the manuscript. The experiments were funded by the Australian Research Council to J.H. Q.Q. has been financially supported by the National Natural Science Foundation of China [41172065, 90914008, 41023009, 40872057] and the Chinese Academy of Sciences (XDB03010201).

References

Adam J, Rushmer T, O'Neil J, Francis D (2012) Hadean greenstones from the Nuvvuagittuq fold belt and the origin of the Earth's early continent crust. Geology 40:363–366

Alonso-Perez R, Müntener O, Ulmer P (2009) Igneous garnet and amphibole fractionation in the roots of island arcs: experimental constraints on andesitic liquids. Contrib Mineral Petrol 157:541–558

Arth JG (1976) Behaviour of trace elements during magmatic processes-a summary of theoretical models and their applications. J Res US Geol Surv 4:41–47

Arth JG, Hanson GN (1972) Quartz diorites derived by partial melting of eclogite or amphibolite at mantle depths. Contrib Mineral Petrol 37:161–174

Atherton MP, Petford N (1993) Generation of sodium-rich magmas from newly underplated basaltic crust. Nature 362:144–146

Beard JS, Lofgren GE (1991) Dehydration melting and water-saturated melting of basaltic and andesitic greenstones and amphibolites at 1, 3, and 6.9 kb. J Petrol 32:365–401

Beate B, Monzier M, Spikings R, Cotton J, Silva J, Bourdon E, Eissen JP (2001) Mio-Pliocene adakite generation related to flat subduction in southern Ecuador: the Quimsacocha volcanic center. Earth Planet Sci Lett 192:561–570

Bedard JH (2006) A catalytic delamination-driven model for coupled genesis of Archaean crust and sub-continental lithospheric mantle. Geochim Cosmochim Acta 70:1188–1214

Blundy J, Wood B (1994) Prediction of crystal-melt partition coefficients from elastic modull. Nature 372:452–454

Bottazzi P, Tiepolo M, Vannucci R, Zanetti A, Brumm R, Foley SF, Oberti R (1999) Distinct site preferences for heavy and light REE in amphibole and the prediction of $^{Amph/L}D_{REE}$. Contrib Mineral Petrol 137:36–45

Brenan JM, Shaw HF, Ryerson FJ, Phinney DL (1995) Experimental determination of trace-element partitioning between pargasite and a synthetic hydrous andesitic melt. Earth Planet Sci Lett 135:1–11

Brey GP, Köhler T (1990) Geothermobarometry in four-phase lherzolites II. New thermobarometers, and practical assessment of existing thermobarometers. J Petrol 31:1353–1378

Bussod GYA, Williams DR (1991) Thermal and kinematic model of the southern Rio Grande rift: inferences from crustal and mantle xenoliths from Kilbourne Hole, New Mexico. Tectonophysics 197:373–389

Chung SL, Liu DY, Ji JQ, Chu MF, Lee HY, Wen DJ, Lo CH, Lee TY, Qian Q, Zhang Q (2003) Adakites from continental collision zones: melting of thickened lower crust beneath southern Tibet. Geology 31:1021–1024

Clemens JD, Stevens G (2012) What controls chemical variation in granitic magmas? Lithos 134–135:317–329

Clemens JD, Yearron LM, Stevens G (2006) Barberton (South Africa) TTG magmas: geochemical and experimental constraints on source-rock petrology, pressure of formation and tectonic setting. Precamb Res 151:53–78

Coldwell B, Clemens J, Petford N (2011) Deep crustal melting in the Peruvian Andes: felsic magma generation during delamination and uplift. Lithos 125:272–286

Condie KC (2005) TTGs and adakites: are they both slab melts? Lithos 80:33–44

Condie KC, Selverstone J (1999) The crust of the Colorado Plateau: new views of an old arc. J Geol 107:387–397

De Wit MJ (1998) On Archean granites, greenstones, cratons and tectonics: does the evidence demand a verdict? Precamb Res 91:181–226

Defant MJ, Drummond MS (1990) Derivation of some modern arc magmas by melting of young subducted lithosphere. Nature 347:662–665

Defant MJ, Xu JF, Kepezhinskas P, Wang Q, Zhang Q, Xiao L (2002) Adakites: some variations on a theme. Acta Petrologica Sinica 18:129–142

Diwu CR, Sun Y, Lin CL, Liu XM, Wang HL (2007) Zircon U-Pb ages and Hf isotopes and their geological significance of Yiyang TTG gneisses from Henan province, China. Acta Petrologica Sinica 23:253–262

Drummond MS, Defant MJ (1990) A model for trondhjemite-tonalite-dacite genesis and crustal growth via slab melting: archean to modern comparisons. J Geophys Res 95:21503–21521

Foley S, Tiepolo M, Vannucci R (2002) Growth of early continental crust controlled by melting of amphibolite in subduction zones. Nature 417:837–840

Fumagalli P, Poli S (2005) Experimentally determined phase relations in hydrous peridotites to 6.5 GPa and their consequences on the dynamics of subduction zones. J Petrol 46:555–578

Gaetani GA, Grove TL (1998) The influence of water on melting of mantle peridotite. Contrib Mineral Petrol 131:323–346

Gao S, Rudnick RL, Yuan HL, Liu XM, Liu YS, Xu WL, Ling WL, Ayers J, Wang XC, Wang QH (2004) Recycling lower continental crust in the North China craton. Nature 432:892–897

Green TH (1982) Anatexis of mafic crust and high pressure crystallization of andesite. In: Thorpe RS (ed) Andesites: orogenic andesites and related rocks. John Wiley & Sons, New York, pp 465–487

Green TH, Pearson NJ (1987) An experimental study of Nb and Ta partitioning between Ti-rich minerals and silicate liquids at high pressure and temperature. Geochim Cosmochim Acta 51:55–62

Grove TL, Donnelly-Nolan JM, Housh T (1997) Magmatic processes that generated the rhyolite of Glass Mountain, Medicine Lake volcano, N. California. Contrib Mineral Petrol 127:205–223

Guo ZF, Wilson M, Liu JQ (2007) Post-collisional adakites in south Tibet: products of partial melting of subduction-modified lower crust. Lithos 96:205–224

Hacker BR, Gnos E, Ratschbacher L, Grove M, McWilliams M, Sobolev SV, Jiang W, Wu ZH (2000) Hot and dry deep crustal xenoliths from Tibet. Science 287:2463–2466

Harrison TM, Watson EB (1984) The behavior of apatite during crustal anatexis: equilibrium and kinetic considerations. Geochim Cosmochim Acta 48:1467–1477

Hayden LA, Watson EB (2007) Rutile saturation in hydrous siliceous melts and its bearing on Ti-thermometry of quartz and zircon. Earth Planet Sci Lett 258:561–568

Helz RT (1976) Phase relations of basalts in their melting ranges at $P_{H2O} = 5$ kb. Part II. Melt compositions. J Petrol 17:139–193

Hermann J (2002) Allanite: thorium and light rare earth element carrier in subducted crust. Chem Geol 192:289–306

Hermnan J, Green DH (2001) Experimental constraints on high pressure melting in subducted crust. Earth Planet Sci Lett 188:149–168

Hibberson WO (1978) High pressure and high temperature techniques as applied to experimental petrology. Sci Technol 15(5):22–23

Hilyard M, Nielsen RL, Beard JS, Patino-Douce A, Blencoe J (2000) Experimental determination of the partitioning behavior of rare earth and high field strength elements between pargasitic amphibole and natural silicate melts. Geochim Cosmochim Acta 64:1103–1120

Hollings P, Kerrich R (2000) An Archean arc basalt-Nb-enriched basalt-adakite association: the 2.7 Ga Confederation assemblage of the Birch-Uchi greenstone belt, Superior Province. Contrib Mineral Petrol 139:208–226

Hou ZQ, Gao YF, Qu XM, Rui ZY, Mo XX (2004) Origin of adakitic intrusives generated during mid-Miocene east-west extension in southern Tibet. Earth Planet Sci Lett 220:139–155

Huang F, Li SG, Dong F, He YS, Chen FK (2008) High-Mg adakitic rocks in the Dabie orogen, central China: implications for foundering mechanism of lower continental crust. Chem Geol 255:1–13

Huang XL, Niu YL, Xu YG, Yang QJ, Zhong JW (2010) Geochemistry of TTG and TTG-like gneisses from Lushan-Taihua complex in the southern North China Craton: implications for late Archean crustal accretion. Precamb Res 182:43–56

Hyndman RD, Currie CA, Mazzotti SP (2005) Subduction zone backarcs, mobile belts, and orogenic heat. GSA Today 15:4–10

Jahn BM, Liu DY, Wang YS, Song B, Wu JS (2008) Archean crustal evolution of the Jiaodong peninsula, China, as revealed by zircon SHRIMP geochronology, elemental and Nd-isotope geochemistry. Am J Sci 308:232–269

Jiang N, Liu YS, Zhou WG, Yang JH, Zhang SQ (2007) Derivation of Mesozoic adakitic magmas from ancient lower crust in the North China craton. Geochim Cosmochim Acta 71:2591–2608

Jiang N, Guo JH, Zhai MG, Zhang SQ (2010) $\sim$2.7 Ga crust growth in the North China craton. Precamb Res 179:37–49

John T, Klemd R, Klemme S, Pfänder JA, Hoffmann JE, Gao J (2011) Nb-Ta fractionation by partial melting at the titantite-rutile transition. Contrib Mineral Petrol 161:35–45

Karsli O, Dokuz A, Uysal I, Aydin F, Kandemir R, Wijbrans J (2010) Generation of the early Cenozoic adakitic volcanism by partial melting of mafic lower crust, Eastern Turkey: implications for crustal thickening to delamination. Lithos 114:109–120

Kay RW (1978) Aleutian magnesian andesites: melts from subducted Pacific Ocean crust. J Volcanol Geotherm Res 4:117–132

Kay RW, Kay SM (2002) Andean adakites: three ways to make them. Acta Petrologica Sinica 18:303–311

Kemp AIS, Hawkesworth CJ, Paterson BA, Kinny PD (2006) Episodic growth of the Gondwana supercontinent from hafnium and oxygen isotopes in zircon. Nature 439:580–583

Kinzler RJ (1997) Melting of mantle peridotite at pressures approaching the spinel to garnet transition: application to mid-ocean ridge basalt petrogenesis. J Geophys Res 102:853–874

Klein M, Stosch HG, Seck HA (1997) Partitioning of high field-strength and rare-earth elements between amphibole and quartz-dioritic to tonalitic melts: an experimental study. Chem Geol 138:257–271

Klein M, Stosch HG, Seck HA, Shimizu N (2000) Experimental partitioning of high field strength and rare earth elements between clinopyroxene and garnet in andesitic to tonalitic systems. Geochim Cosmochim Acta 64:99–115

Klemme S, Blundy JD, Wood BJ (2002) Experimental constraints on major and trace element partitioning during partial melting of eclogite. Geochim Cosmochim Acta 66:3109–3123

Koepke J, Falkenberg G, Rickers K, Diedrich O (2003) Trace element diffusion and element partitioning between garnet and andesite melt using synchrotron X-ray fluorescence microanalysis (μ-SRXRF). Eur J Mineral 15:883–892

Lambert IB, Wyllie PJ (1972) Melting of gabbro (quartz eclogite) with excess water to 35 kilobars, with geological applications. J Geol 80:693–708

Laurie A, Stevens G (2012) Water-present eclogite melting to produce Earth's early felsic crust. Chem Geol 314–317:83–95

Liu J, Bohlen SR, Ernst WG (1996) Stability of hydrous phases in subducting oceanic crust. Earth Planet Sci Lett 143:161–171

Liu YS, Gao S, Jin SY, Hu SH, Sun M, Zhao ZB, Feng JL (2001) Geochemistry of lower crustal xenoliths from Neogene Hannuoba basalt, North China Craton: implications for petrogenesis and lower crustal composition. Geochim Cosmochim Acta 65:2589–2604

Liu YS, Gao S, Liu XM, Chen XM, Zhang WL, Wang XC (2003) Thermodynamic evolution of lithosphere of the North China craton: records from lower crust and upper mantle xenoliths from Hannuoba. Chin Sci Bull 48:2371–2377

Liu SW, Pan YM, Xie QL, Zhang J, Li QG (2004) Archean geodynamics in the Central Zone, North China Craton: constraints from geochemistry of two contrasting series of granitoids in the Fuping and Wutai complexes. Precamb Res 130:229–249

Liu SA, Li SG, He YS, Huang F (2010) Geochemical constraints between early cretaceous ore-bearing and ore-barren high-Mg adakites in central-eastern China: implications for petrogenesis and Cu-Au mineralization. Geochim Cosmochim Acta 74:7160–7178

Lopez S, Castro A (2001) Determination of the fluid-absent solidus and supersolidus phase relationships of MORB-derived amphibolites in the range 4–14 kbar. Am Mineral 86:1396–1403

Macpherson CG, Dreher ST, Thirlwall MF (2006) Adakites without slab melting: high pressure differentiation of island arc magma, Mindanao, the Philippines. Earth Planet Sci Lett 243:581–593

Martin H (1986) Effect of steeper Archean geothermal gradient on geochemistry of subduction-zone magmas. Geology 14:753–756

Martin H (1987) Petrogenesis of Archaean trondhjemites, tonalites, and granodiorites from Eastern Finland: major and trace element geochemistry. J Petrol 28:921–953

Martin H (1999) Adakitic magmas: modern analogues of Archaean granitoids. Lithos 46:411–429

Martin H, Moyen JF (2002) Secular changes in tonalite—trondhjemite—granodiorite composition as markers of the progressive cooling of earth. Geology 30:319–322

Martin H, Smithies RH, Rapp R, Moyen JF, Champion D (2005) An overview of adkaite, tonalite-trondhjemite-granodiorite (TTG), and sanukitoid: relationships and some implications for crustal evolution. Lithos 79:1–24

Morris PA (1995) Slab melting as an explanation of quaternary volcanism and aseismicity in southwest Japan. Geology 23:395–398

Moyen JF (2009) High Sr/Y and La/Yb ratios: the meaning of the "adakitic" signature. Lithos 112:556–574

Moyen JF (2011) The composite Archaean grey gneisses: petrological significance, and evidence for a non-unique tectonic setting for Archaean crustal growth. Lithos 123:21–36

Moyen JF, Stevens G, Kisters AFM, Belcher RW (2007) TTG plutons of the Barberton granitoid-greenstone terrain, South Africa. In: Martin J, Kranindonk V, Smithies H, Bennett VC (ed) Earth's Oldest Rocks. Developments in Precambrian Geology, Elsevier, pp 607–667

Muir RJ, Weaver SD, Bradshaw JD et al (1995) The cretaceous separation point batholith, New Zealand: granitoid magmas formed by melting of mafic lithosphere. J Geol Soc Lond 152:689–701

Nagel TJ, Hoffmann JE, Münker C (2012) Generation of Eoarchean tonalite-trondhjemite-granodiorite series from thickened mafic arc crust. Geology 40:375–378

Nair R, Chacko T (2008) Role of oceanic plateaus in the initiation of subduction and origin of continental crust. Geology 36:583–586

Nakajima K, Arima M (1998) Melting experiments on hydrous low-K tholeiite: implications for the genesis of tonalitic crust in the Izu-Bonin-Mariana arc. Island Arc 7:359–373

Nath WP, Crecraft HR (1985) Partition coefficients for trace elements in silicic magmas. Geochim Cosmochim Acta 49:2309–2322

Nehring F, Foley SF, Hölttä P, van den Kerkhof AM (2009) Internal differentiation of the Archean continental crust: fluid-controlled partial melting of granulites and TTG-amphibolite associations in Central Finland. J Petrol 50:3–35

Nehring F, Foley SF, Hölttä P (2010) Trace element partitioning in the granulite facies. Contrib Mineral Petrol 159:493–519

O'Reilly SY, Griffin WL (1985) A xenolith-derived geotherm for southeastern Australia and its geophysical implications. Tectonophysics 111:41–63

Patino Douce AE, Beard JS (1995) Dehydration-melting of biotite gneiss and quartz amphibolite from 3 to 15 kbar. J Petrol 36:707–738

Peacock SM, Rushmer T, Thompson AB (1994) Partial melting of subducting oceanic crust. Earth Planet Sci Lett 121:227–244

Pearce NJG, Perkins WT, Westgate JA, Gorton MP, Jackson SE, Neal CR, Chenery SP (1997) A compilation of new and published major and trace element data for NIST SRM 610 and NIST SRM 612 glass reference materials. Geostandards Newsl 21:115–144

Petford N, Atherton M (1996) Na-rich partial melts from newly underplated basaltic crust: the Cordillera Blanca Batholith, Peru. J Petrol 37:1491–1521

Philpotts JA, Schnetzler CC (1970) Phenocryst-matrix partition coefficients for K, Rb, Sr and Ba, with applications to anorthosite and basalt genesis. Geochim Cosmochim Acta 34:307–322

Polat A, Kerrich R (2001) Magnesian andesites, Nb-enriched basalt-andesites, and adakites from late-Archean 2.7 Ga Wawa greenstone belts, Superior Province, Canada: implications for late Archean subduction zone petrogenetic processes. Contrib Mineral Petrol 141:36–52

Polat A, Kusky T, Li JH, Fryer B, Kerrich R, Patrick K (2005) Geochemistry of Neoarchean (ca. 2.55–2.50 Ga) volcanic and ophiolitic rocks in the Wutaishan greenstone belt, central orogenic belt, North China craton: implications for gendynamic setting and continental growth. GSA Bull 117:1387–1399

Qian Q, Hermann J (2010) Formation of high-Mg diorites through assimilation of Peridotite by monzodiorite magma at crustal depths. J Petrol 51:1381–1416

Rapp RP (1995) Amphibole-out phase boundary in partially melted metabasalt, its control over liquid fraction and composition, and source permeability. J Geophys Res 100(B8):15601–15610

Rapp RP, Watson EB (1995) Dehydration melting of metabasalt at 8–32 kbar: implications for continental growth and crust-mantle recycling. J Petrol 36:891–931

Rapp RP, Watson EB, Miller CF (1991) Partial melting of amphibolite/eclogite and the origin of Archean trondhjemites and tonalities. Precamb Res 51:1–25

Rapp RP, Shimizu N, Norman MD, Applegate GS (1999) Reaction between slab-derived melts and peridotite in the mantle wedge: experimental constraints at 3.8 GPa. Chem Geol 160:335–356

Rapp RP, Xiao L, Shimizu N (2002) Experimental constraints on the origin of potassium-rich adakites in eastern China. Acta Petrologica Sinica 18:293–302

Rapp RP, Shimizu N, Norman MD (2003) Growth of early continental crust by partial melting of eclogite. Nature 425:605–609

Rollinson H (2012) Geochemical constraints on the composition of Archaean lower continental crust: partial melting in the Lewisian granulites. Earth Planet Sci Lett 351–352:1–12

Rubatto D, Hermann J (2007) Experimental zircon/melt and zircon/garnet trace element partitioning and implications for the geochronology of crustal rocks. Chem Geol 241:38–61

Rudnick RL, Gao S (2003) Composition of the continental crust. In: Rudnick RL, Holland HD, Turekian KK (eds) Treatise on geochemistry, vol 3, the crust, Elsevier, pp 1–64

Rushmer T (1991) Partial melting of two amphibolites: contrasting experimental results under fluid-absent conditions. Contrib Mineral Petrol 107:41–59

Ryerson FJ, Watson EB (1987) Rutile saturation in magmas: implications for Ti-Nb-Ta depletion in island-arc basalts. Earth Planet Sci Lett 86:225–239

Sage RP, Lightfoot PC, Doherty W (1996) Geochemical characteristics of granitoid rocks from within the Archean Michipicoten Greenstone Belt, Wawa Subprovince, Superior Province, Canada: implications for source regions and tectonic evolution. Precamb Res 76:155–190

Sajona FG, Maury RC, Bellon H, Cotton J, Defant MJ, Pubellier M (1993) Initiation of subduction and the generation of slab melts in western and eastern Mindanao, Philippines. Geology 21:1007–1010

Schnetzler CC, Philpotts JA (1970) Partition coefficients of rare earth elements between igneous matrix material and rock-forming mineral phenocrysts-II. Geochim Cosmochim Acta 34:331–340

Sen C, Dunn T (1994) Dehydration melting of a basaltic composition amphibolite at 1.5 and 2.0 GPa: implications for the origin of adakites. Contrib Mineral Petrol 117:394–409

Severs MJ, Beard JS, Fedele L, Hanchar JM, Mutchler SR, Bodnar RJ (2009) Partitioning behavior of trace elements between dacitic melt and plagioclase, orthopyroxene, and clinopyroxene based on laser ablation ICPMS analysis of silicate melt inclusions. Geochim Cosmochim Acta 73:2123–2141

Shannon RD (1976) Revised effective ionic radii and systematic studies of interatomic distances in halides and chacogenides. Acta Crystallogr A32:751–767

Sisson TW (1994) Hornblende-melt trace-element partitioning measured by ion microprobe. Chem Geol 117:331–344

Sisson TW, Grove TL (1993) Experimental investigations of the role of H_2O in calc-alkaline differentiation and subduction zone magmatism. Contrib Mineral Petrol 113:143–166

Sisson TW, Ratajeski K, Hankins WB, Glazner AF (2005) Voluminous granitic magmas from common basaltic sources. Contrib Mineral Petrol 148:635–661

Skjerlie KP, Patino Douce AE (2002) The fluid-absent partial melting of a zoisite-bearing quartz eclogite from 1.0 to 3.2 GPa; Implications for melting in thickened continental crust and for subduction-zone processes. J Petrol 43:291–314

Smithies RH (2000) The Archaean tonalite-trondhjemite-granodiorite (TTG) series is not an analogue of Cenozoic adakite. Earth Planet Sci Lett 182:115–125

Smithies RH, Champion DC, Cassidy KF (2003) Formation of Earth's early Archaean continental crust. Precamb Res 127:89–101

Smithies RH, Champion DC, Van Kranendonk MJ (2009) Formation of Paleoarchean continental crust through infracrustal melting of enriched basalt. Earth Planet Sci Lett 281:298–306

Springer W, Seck HA (1997) Partial fusion of basic granulites at 5 to 15 kbar: implications for the origin of TTG magmas. Contrib Mineral Petrol 127:30–45

Stern CR, Kilian R (1996) Role of the subducted slab, mantle wedge and continental crust in the generation of adakites from the Andean Austral Volcanic Zone. Contrib Mineral Petrol 123:263–281

Stimac J, Hickmott D (1994) Trace-element partition coefficients for ilmenite, orthopyroxene and pyrrhotite in rhyolite determined by micro-PIXE analysis. Chem Geol 117:313–330

Storkey AC, Hermann J, Hand M, Buick IS (2005) Using in situ trace-element determinations to monitor partial-melting processes in metabasites. J Petrol 46:1263–1308

Sun SS, McDonough WF (1989) Chemical and isotopic systematics of oceanic basalts: implications for mantle composition and processes. In: Saunders AD, Norry MJ (eds) Magmatism in the Ocean Basins, vol 42. Geological Society, London, pp 313–345

Thompson AB, Ellis DJ (1994) $CaO + MgO + Al_2O_3 + SiO_2 + H_2O$ to 35 kb: amphibole, talc, and zoisite dehydration and melting reactions in the silica-excess part of the system and their possible significance in subduction zones, amphibolite melting, and magma fractionation. Am J Sci 294:1229–1289

Tiepolo M, Oberti R, Zanetti A, Vannucci R, Foley SF (2007) Trace-element partitioning between amphibole and silicate melt. Rev Mineral Geochem 67:417–452

Turkina OM, Berezhnaya NG, Larionov AN, Lepekhina EN, Presnyakov SL, Saltykova TE (2009) Paleoarchean tonalite-trondhjemite complex in the northwestern part of the Sharyzhalgai uplift (southwestern Siberian craton): results of U-Pb and Sm-Nd study. Russ Geol Geophys 50:15–28

van Westrenen W, Blundy JD, Wood BJ (2001) High field strength element/rare earth element fractionation during partial melting in the presence of garnet: implications for identification of mantle heterogeneities. Geochem Geophys Geosys 2: paper 2000GC00133

Wang Q, McDermott F, Xu JF, Bellon H, Zhu YT (2005) Cenozoic K-rich adakitic volcanic rocks in the Hohxil area, northern Tibet: lower-crustal melting in an intracontinental setting. Geology 33:465–468

Wang Q, Xu JF, Jian P, Bao ZW, Zhao ZH, Li CF, Xiong XL, Ma JL (2006) Petrogenesis of adakitic porphyries in an extensional tectonic setting, Dexing, South China: implications for the genesis of porphyry copper mineralization. J Petrol 47:119–144

Wang Q, Wyman DA, Xu JF, Jian P, Zhao ZH, Li CF, Xu W, Ma JL, He B (2007) Early Cretaceous adakitic granites in the Northern Dabie complex, central China: implications for partial melting and delamination of thickened lower crust. Geochim Cosmochim Acta 71:2609–2636

Watson EB, Harrison TM (1983) Zircon saturation revisited: temperature and composition effects in a variety of crustal magma types. Earth Planet Sci Lett 64:295–304

Whalen JB, Percival JA, McNicoll VJ, Longstaffe FJ (2002) A mainly crustal origin for tonalitic granitoid rocks, Superior Province, Canada: implications for late Archean tectonomagmatic processes. J Petrol 43:1551–1570

Whalen JB, Percival JA, McNicoll VJ, Longstaffe FJ (2004) Geochemical and isotopic (Nd-O) evidence bearing on the origin of late- to post-orogenic high-K granitoid rocks in the Western Superior Province: implications for late Archean tectonomagmatic processes. Precamb Res 132:303–326

Wilke M, Behrens H (1999) The dependence of the partitioning of iron and europium between plagioclase and hydrous tonalitic melt on oxygen fugacity. Contrib Mineral Petrol 137:102–114

Winther KT (1996) An experimentally based model for the origin of tonalitic and trondhjemitic melts. Chem Geol 127:43–59

Winther KT, Newton RC (1991) Experimental melting of hydrous low-K tholeiite: evidence on the origin of Archaean cratons. Bull Geo Soc Denmark 39:213–228

Wolf MB, Wyllie PJ (1994) Dehydration-melting of amphibolite at 10 kbar: the effects of temperature and time. Contrib Mineral Petrol 115:369–383

Wood BJ, Banno S (1973) Garnet-orthopyroxene and orthopyroxene-clinopyroxene relationships in simple and complex systems. Contrib Mineral Petrol 42:109–124

Wyllie PJ, Wolf MB (1993) Amphibolite dehydration-melting: sorting out the solidus. In: Alabaster HM, Harris NBW, Neary CR (eds) Magmatic processes and plate tectonics. Geological Society Special Publication, No 76, pp 405–416

Xiao L, Clemens JD (2007) Origin of potassic (C-type) adakite magmas: experimental and field constraints. Lithos 95:399–414

Xiong XL (2006) Trace element evidence for growth of early continental crust by melting of rutile-bearing hydrous eclogite. Geology 34:945–948

Xiong XL, Adam J, Green TH (2005) Rutile stability and rutile/melt HFSE partitioning during partial melting of hydrous basalt: implications for TTG genesis. Chem Geol 218:339–359

Xiong XL, Keppler H, Audetat A, Gudfinnsson G, Sun WD, Song MS, Xiao WS, Yuan L (2009) Experimental constraints on rutile saturation during partial melting of metabasalt at the amphibolite to eclogite transition, with applications to TTG genesis. Am Mineral 94:1175–1186

Xu JF, Shinjo R, Defant MJ, Wang Q, Rapp RP (2002) Origin of Mesozoic adakitic intrusive rocks in the Ningzhen area of east China: partial melting of delaminated lower continental crust? Geology 30:1111–1114

Xu WL, Wang QH, Wang DY, Guo JH, Pei FP (2006) Mesozoic adakitic rocks from the Xuzhou-Suzhou area, eastern China: evidence for partial melting of delaminated lower continental crust. J Asian Earth Sci 27:230–240

Xu WL, Hergt JM, Gao S, Pei FP, Wang W, Yang DB (2008) Interaction of adakitic melt-peridotite: implications for the high-Mg# signature of Mesozoic adakitic rocks in the eastern North China Craton. Earth Planet Sci Lett 265:123–137

Xu WL, Yang DB, Gao S, Pei FP, Yu Y (2010) Geochemistry of peridotite xenoliths in early cretaceous high-Mg# diorites from the Central Orogenic Block of the North China Craton: the nature of Mesozoic lithospheric mantle and constraints on lithospheric thinning. Chem Geol 270:257–273

Yu SY, Zhang JX, Del Real PG (2012) Geochemistry and zircon U-Pb ages of adakitic rocks from the Dulan area of the North Qaidam UHP terrane, north Tibet: constraints on the timing and nature of regional tectonothermal events associated with collisional orogeny. Gondwana Res 21:167–179

Zegers TE, van Keken PE (2001) Middle Archean continent formation by crustal delamination. Geology 29:1083–1086

Zhang Q, Qian Q, Wang EQ, Wang Y, Zhao TP, Hao J, Guo GJ (2001) An East China Plateau in mid-late Yanshanian period: implication from adakites. Chinese J Geol 36:248–255 (in Chinese with English abstract)

Zhang HF, Parrish R, Zhang L, Xu WC, Yuan HL, Gao S, Crowley QG (2007) A-type granite and adakitic magmatism association in Songpan-Garze fold belt, eastern Tibetan Plateau: implication for lithospheric delamination. Lithos 97:323–335

Zhang C, Ma CQ, Holtz F (2010) Origin of high-Mg adakitic magmatic enclaves from the Meichuan pluton, southern Dabie orogen (central China): implications for delamination of the lower continental crust and melt-mantle interaction. Lithos 119:467–484

Zhao ZH, Xiong XL, Wang Q, Wyman DA, Bao ZW, Bai ZH, Qiao YL (2008) Underplating-related adakites in Xinjiang Tianshan, China. Lithos 102:374–391